Atmospheric
Chemistry
and Physics
Discussions

1 **Investigation of global nitrate from the AeroCom Phase III experiment**
2
3 Huisheng Bian[1,2], Mian Chin[2], Didier A. Hauglustaine[3], Michael Schulz[4], Gunnar Myhre[5,6],
4 Susanne E. Bauer[7,8], Marianne T. Lund[6], Vlassis A. Karydis[9], Tom L. Kucsera[10], Xiaohua Pan[11],
5 Andrea Pozzer[9], Ragnhild B. Skeie[6], Stephen D. Steenrod[10], Kengo Sudo[12], Kostas
6 Tsigaridis[7,8], Alexandra P. Tsimpidi[9], and Svetlana G. Tsyro[4]
7
8 [1] Joint Center for Environmental Technology UMBC, Baltimore, MD, USA
9 [2] Laboratory for Atmospheres, NASA Goddard Space Flight Center, Greenbelt, MD, USA
10 [3] Laboratoire des Sciences du Climat et de l'Environnement (LSCE), UMR8212, CEA-CNRS-UVSQ, Gif-
11 sur-Yvette, France
12 [4] Norwegian Meteorological Institute, Blindern, Norway
13 [5] Department of Geosciences, University of Oslo, Oslo, Norway
14 [6] Center for International Climate and Environmental Research-Oslo, Oslo, Norway
15 [7] The Earth Institute, Center for Climate Systems Research, Columbia University, New York, USA
16 [8] NASA Goddard Institute for Space Studies, New York, USA
17 [9] Max Planck Institute for Chemistry, 55128 Mainz, Germany
18 [10] Universities Space Research Association, GESTAR, Columbia, MD, USA
19 [11] School of Computer, Mathematical and Natural Sciences, Morgan State University, Baltimore, MD, USA
20 [12] Center for Climate System Research, University of Tokyo, Tokyo, Japan.
21
22 **Abstract**
23 An assessment of global nitrate and ammonium aerosol based on simulations from nine
24 models participating in the AeroCom Phase III study is presented. A budget analyses was
25 conducted to understand the typical magnitude, distribution, and diversity of the aerosols
26 and their precursors among the models. To gain confidence on model performance, the
27 model results were evaluated with various observations globally, including ground station
28 measurements over North America, Europe, and East Asia for tracer concentrations and
29 dry and wet depositions, as well as with aircraft measurements in the Northern
30 Hemisphere mid-high latitudes for tracer vertical distributions. Given the unique
31 chemical and physical features of the nitrate occurrence, we further investigated the
32 similarity and differentiation among the models by examining: 1) the pH-dependent NH_3
33 wet deposition; 2) the nitrate formation via heterogeneous chemistry on the surface of
34 dust and sea-salt particles; and 3) the nitrate coarse mode fraction (i.e., coarse/total). It is
35 found that HNO_3, which is simulated explicitly based on full O_3-HO_x-NO_x-aerosol
36 chemistry by all models, differs by up to a factor of 9 among the models in its global
37 tropospheric burden. This partially contributes to a large difference in NO_3^-, whose
38 atmospheric burden differs by up to a factor of 13. Analyses at the process level show
39 that the large diversity in atmospheric burdens of NO_3^-, NH_3, and NH_4^+ is also related to
40 deposition processes. Wet deposition seems to be the dominant process in determining
41 the diversity in NH_3 and NH_4^+ lifetimes. It is critical to correctly account for contributions
42 of heterogeneous chemical production of nitrate on dust and sea-salt, because this process
43 overwhelmingly controls atmospheric nitrate production (typically >80%) and determines
44 the coarse and fine mode distribution of nitrate aerosol.
45
46 **1. Introduction**
47 Atmospheric aerosols adversely affect human health and play an important role in
48 changing the Earth's climate. A series of multimodel studies have been coordinated by
49 the international activity of Aerosol Comparisons between Observations and Models

Atmospheric
Chemistry
and Physics
Discussions

Open Access

EGU

50   (AeroCom) in its Phase I and II model experiments that have systematically assessed the
51   presence and influence of almost all major atmospheric anthropogenic and natural
52   aerosols (such as sulfate, dust, and carbonaceous aerosols) (e.g., Kinne et al., 2006;
53   Schulz et al., 2006; Textor et al., 2006; Koch et al., 2009; Huneeus et al., 2011; Tsigaridis
54   et al., 2014; Kim et al., 2015). Very little attention has been drawn to nitrate aerosol other
55   than its contribution to radiative forcing (Myhre et al., 2013). One obvious reason is that
56   not many models used to include nitrate owing to the chemical complexity of nitrate
57   formation. However, atmospheric nitrate aerosol not only exerts direct effects on air
58   quality and climate, but also uniquely impacts the Earth system by being directly
59   involved in tropospheric chemistry and constraining net primary productivity, hence
60   altering carbon sequestration and ecological effects, via its deposition (Prentice et al.,
61   2001).
62
63   Atmospheric nitrate contributes notably to total aerosol mass in the present-day,
64   especially in urban areas and agriculture regions. Nitrate is about a quarter of sulfate in
65   terms of overall global burden, AOD, and direct forcing at the present-day according to
66   the study of AeroCom II direct forcing experiment (Myhre et al., 2013). This conclusion
67   is confirmed by recent publications using various individual models and emission
68   inventories (Bellouin et al; 2011; Bauer et al., 2007; Hauglustaine 2014; Karydis et al.,
69   2016; Mezuman et al., 2016; Paulot et al., 2016). Regionally, considerable evidences
70   from in-situ measurements (Bessagnet et al., 2014; Haywood et al., 2008; Jimenez et al.,
71   2009; Malm et al., 1994; Vieno et al., 2016) and model results (Karydis et al., 2011;
72   Ensberg et al., 2013; Trump et al., 2015) indicate that nitrate becomes one of the major
73   aerosol species in urban and agriculture environments. For example, nitrate concentration
74   is about half of sulfate during the summer season in Beijing (Zhou et al., 2016) and
75   represents a large portion of wintertime aerosol mass in the San Joaquin Valley in
76   California (Pusede et al., 2016).
77
78   More importantly, the importance of aerosol nitrate is likely to increase over the century
79   with a projected decline in SO_2 and NO_x emissions and increase in NH_3 emissions (IPCC,
80   2013). With the reduction of SO_2 emissions, less atmospheric NH_3 is required to
81   neutralize the strong acid H_2SO_4. The excess of NH_3 results in gaseous HNO_3 and NH_3
82   entering the condensed phase, and their subsequent dissociation yields nitrate and
83   ammonium ions. The trend of future nitrate depends on which is the limited species, NO_x
84   or NH_3, for nitrate formation (Tsimpidi et al., 2007; 2008). Generally, our atmosphere, at
85   its current and foreseeable near future, is still in an NH_3-limited condition according to
86   sensitivity studies by Heald et al. (2012) and Walker et al. (2012). Almost all global
87   models predicted an overall increase of atmospheric nitrate burden during this century
88   based on current available emission inventories (Bauer et al 2007; 2016; Bellouin et al.,
89   2011; Hauglustaine et al., 2014; Li et al., 2014). For example, using CMIP5 future
90   emission projections, Bellouin et al. (2011) concluded that, by 2090, nitrate would
91   become an important aerosol species in Europe and Asia, contributing up to two thirds of
92   the globally averaged anthropogenic optical depth. However, the predicted trend of
93   surface nitrate is mixed. Some studies estimated a consistent increase of surface nitrate
94   (Bellouin et al., 2011), while others pointed out that this increase might vanish or even
95   reverse over some regional urban areas due to the decline of NO_x emissions (Bauer et al.,

Atmospheric
Chemistry
and Physics
Discussions

96   2016; Pusede et al., 2016; Trail et al., 2014). Nevertheless, the potentially increasing
97   importance of nitrate in climate and its large uncertainty in future surface nitrate
98   predictions urge us to characterize model performance and understand the
99   physicochemical mechanisms behind the diversity of nitrate simulations.
100
101 Nitrate is also important in that its formation directly affects tropospheric chemistry.
102 First, the formation of nitrate, through either aqueous phase chemical reaction between
103 HNO_3 and NH_3 (Metzger et al., 2002; Kim et al., 1993) or heterogeneous reaction of
104 nitrogen species such as HNO_3, NO_3, and N_2O_5 on the surface of dust and sea salt aerosol
105 particles (Bauer et al., 2004; 2005; Bian et al., 2003; Dentener 1996; Liao et al., 2003),
106 converts gas phase nitrogen species into aerosols. Consequently, the global tropospheric
107 NO_x concentration and the rate of conversion of N_2O_5 to HNO_3 will be reduced (Riemer
108 et al., 2003), which in turn leads to the reduction of atmospheric oxidants. For example,
109 global tropospheric O_3 can be reduced by 5% (Bauer et al., 2007) and tropical Atlantic
110 OH by 10% (Bian et al., 2003) just through the heterogeneous reactions of nitrogen
111 radicals on dust. Second, the most important removal path for nitrogen from the
112 atmosphere is the formation of HNO_3, which is subsequently deposited (Riemer et al.,
113 2003). Since HNO_3 is subject to partitioning between the gas and aerosol phases, the
114 lifetimes of nitrogen species can be shortened by the formation of tropospheric nitrate
115 aerosol because the loss of total HNO_3 will be accelerated by a much higher dry
116 deposition in the aerosol phase.
117
118 Large nitrogen deposition occurs over both land and ocean (Dentener et al., 2006;
119 Kanakidou et al., 2012; 2016). Nitrogen deposition can either benefit or impair ecosystem
120 productivity depending on the initial balance of nutrients since different ecosystems have
121 different Nr (reactive nitrogen) availability and retention (Galloway et al., 2004; Prentice
122 et al., 2001). If fixed Nr is deposited as nitrate in forests, it may act as a "fertilizer,"
123 stimulating growth and thus enhancing carbon sequestration (Fowler et al., 2015). But
124 when the accumulated deposition exceeds the nutritional needs of the ecosystem, nitrogen
125 saturation may result (Fenn et al., 1996). Soil fertility declines due to the leeching of
126 cations (Milegroet and Cole, 1984) and, thus, carbon uptake diminishes. The balance
127 between fertilization and saturation depends on the spatial and temporal extent of
128 nitrogen deposition. In order to determine the extent to which the emissions of air
129 pollutants will have to be reduced and whether the environment needs to be protected
130 from damage, it is essential to know where and by how much N deposition exceeds
131 nature's tolerance (Dentener et al. 2006; Lamarque et al., 2005; Phoenix et al., 2006).
132
133 Here we present a nitrate-focused study that has been organized as a part of the series of
134 AeroCom phase III experiments (https://wiki.met.no/aerocom/phase3-experiments). The
135 goals of this activity are to (1) address the diversity of the nitrate simulation by the
136 AeroCom multi-models and diagnose the driving processes for the diversity, (2) explore
137 the uncertainty of the model nitrate simulations constrained against various
138 measurements from ground station networks and aircraft campaigns, and (3) investigate
139 how the formation of nitrate changes in different models in response to perturbation on
140 key precursors and factors that determine nitrate formation. We focus on the first two
141 objectives in this paper. Such a study directs us on how to improve the representation of

Atmospheric
Chemistry
and Physics
Discussions

142   nitrate aerosol formation and size distribution in climate chemistry models and reveals
143   nitrate effects on global air quality and climate.
144
145   Building upon the analysis of the multi-model diversity, three additional sensitivity
146   experiments are designed using the GMI model to further explore the potential sources
147   for the diversity on physical and chemical process-level. First, we explore the impact of
148   pH-dependent NH_3 wet deposition on atmospheric NH_3 and associated nitrogen species.
149   We then reveal the importance of mineral dust and sea salt in the nitrate formation and
150   check the resultant nitrate aerosol size distribution that is particularly important in nitrate
151   forcing estimation.
152
153   The paper is organized as follows. Section 2 introduces the experiment setup including
154   the used emission inventories and the participating Aerocom models. Observations of
155   surface tracer concentrations and dry and wet depositions over U.S., Europe, and East
156   Asia, as well as aircraft measurements in the ARCTAS campaigns are described in
157   section 3. We present AeroCom model inter-comparison and the model evaluation using
158   aforementioned observations in section 4. Based on the knowledge from previous
159   sections, we further discuss nitrate formation in response to physiochemical
160   methodologies in section 5 and summarize our major findings in section 6.
161
162   **2. Experiment setup and AeroCom model description**
163
164   **2.1 Experiment setup**
165   The AeroCom III nitrate experiment comprises one baseline and six perturbation
166   simulations, with the latter designed for assessing the possible future changes of emission
167   and meteorological fields relevant to nitrate formation. Models are advised to use the
168   same prescribed emission datasets for gases and aerosols. Emissions from anthropogenic,
169   aircraft, and ship are obtained from the recently developed HTAP v2 database (Janssens-
170   Maenhout et al., 2015) that provides high spatial resolution monthly emission. For the
171   tracers that are included in ozone chemistry but are not provided by HTAP v2 (i.e. some
172   volatile organic compounds), they should be obtained from CMIP5 RCP85 with a linear
173   interpolation between 2005 and 2010. Biomass burning emissions are the emissions of
174   GFED3 (Werf et al., 2010) in 2008 [http://www.globalfiredata.org/data.html]. The NH_3
175   emission from ocean is adopted based on the compilation of GEIA emission inventory
176   [Bouwman et al., 1997]. Participating modeling groups use their own emissions of
177   dimenthyl sulfide (DMS), dust, sea salt, and NO from lightning, since they are calculated
178   based on models' meteorological fields.
179
180   A full year simulation for 2008 is required for the nitrate model experiment. There are
181   several in-situ observation datasets available in 2008 for model evaluation, including the
182   surface concentration and deposition measurements over the US (CastNet, AMoN,
183   NDAP/NTN), Europe (EMEP), and Asia (EANET), and the aircraft measurements of
184   vertical profiles (e.g. ARCTAS-A, ARCTAS-CARB, and ARCTAS-B). All participating
185   models are required to use the reanalysis or nudged meteorological data for 2008 and
186   allow several months spin up for the baseline simulation.
187

Atmospheric
Chemistry
and Physics
Discussions

2.2 AeroCom models

188
189   Nine models participate in the AeroCom III nitrate experiment. Their general nitrate-
190   related physiochemical mechanisms are summarized in Table 1. Further detailed
191   information on their thermodynamic equilibrium model (TEQM) is given in Table 2.
192
193   The models participating in this study are divided into two groups. Group one (CHASER,
194   EMAC, INCA, GISS-MATRIX, and GISS-OMA) run chemical fields together with
195   meteorological fields, while group two (EMEP, GMI, OsloCTM2, and OsloCTM3)
196   simulate chemical fields using archived meteorological fields. Most models in this study
197   have a horizontal resolution around 2-3 degrees except EMEP with 0.5 degree.
198   Vertically, most models cover both the troposphere and the stratosphere with a peak
199   altitude up to 0.01 hPa except EMEP that extends vertically up to 100 hPa into the
200   troposphere only.
201
202   All models use full gas phase O_3-NO_x-HO_x chemistry to produce HNO_3 and consider the
203   feedback of nitrate aerosol formation on HNO_3 calculation. However, due to the
204   complexity of chemical mechanisms for organic nitrate compounds and different
205   recommendations for reaction rates, HNO_3 fields produced by the models differ greatly.
206   This difference propagates into the subsequent gas-aerosol reactions for nitrate formation.
207
208   These models are very different in their approaches on gas-aerosol reactions in nitrate
209   formation. All models consider reactions between NH_3 and HNO_3. However, models
210   differ dramatically in whether to include heterogeneous reactions on dust and sea salt
211   (Table 1). Some account for both, some for only dust or sea salt, and some do not account
212   for any of them at all. The methods used by the models in accounting for NH_3 and
213   dust/sea salt contributions are also different.
214
215   All participating models adopt TEQM to deal with aqueous and solid phase reactions and
216   gas-aerosol partitioning (Tables 1 and 2). This is based on the assumption that volatile
217   species in the gas and aerosol phases are generally in chemical equilibrium. However, the
218   assumption is not always warranted in some cases, as we will discuss in section 5.2. Even
219   with the TEQM approach, nitrate calculation could differ due to treatments of
220   equilibrium constants or chemical potentials, solute activity coefficients, water activity,
221   and relative humidity of deliquescence (RHD). The parameterizations adopted by the
222   models to deal with multicomponent activity coefficient, binary activity coefficient, and
223   water activity are given in table 2. GISS-OMA, Oslo-CTM2 and Oslo-CTM3 are special
224   in that they assume aerosols to be metastable so that the model does not take into account
225   formation of solids in this study. All other models do consider the effect of the hysteresis
226   of particle phase transitions. All models also assume that the overall particles are large
227   enough to neglect the Kelvin effect.
228
229   The participating models call the TEQMs in different ways to account for aerosol size
230   effect. All the TEQMs (ISORROPIA-I, ISORROPIA-II, MARS, RPMIRES, INCA, and
231   EQSAM3) assume particles to be internally mixed, i.e. all particles of the same size have
232   the same composition. However, some parent models (CHASER, EMEP, GMI, INCA,
233   GISS-MATRIX and GISS-OMA) call their TEQMs only once for fine mode aerosol

Atmospheric
Chemistry
and Physics
Discussions

234   particles, while the others (EMAC, OsloCTM2 and OsloCTM3) call their TEQMs from
235   different aerosol size bins. For example, Oslo-CTM2 and Oslo-CTM3 consider a bi-
236   modal aerosol size-spectrum with two major aerosol modes, fine and coarse, and
237   calculate gas-aerosol equilibrium partitioning with EQSAM3 first for fine mode and then
238   for coarse mode. Additionally, to account for kinetic limitations, EMAC calculates the
239   phase partitioning in two stages. In the first stage, the amount of the gas-phase species
240   that is able to kinetically condense onto the aerosol phase within the model time step is
241   calculated, while in the second stage, the TEQM redistributes the mass between the two
242   phases assuming instant equilibrium (Pringle et al., 2010).
243
244   The TEQMs also differ in the chemical components considered. Specifically, the TEQMs
245   in CHASE, EMEP, GISS-MATRIX, GISS-OMA, GMI and INCA include only species
246   of sulfate, nitrate, ammonium and their gas, liquid, and solid components. The models
247   Oslo-CTM2 and Oslo-CTM3 add NaCl and HCl, while the model EMAC further expands
248   the species by including dust-related crustal material such as Ca^{2+}, K^+, and Mg^{2+}.
249
250   These TEQMs differ in their computational approaches as well. Computational efficiency
251   is a prime consideration for a TEQM that is designed for incorporation into a global air
252   quality and climate study. To speed up the calculation, TEQMs typically divide the
253   system into sub-domains based on RH and concentrations of ammonium, sodium, crustal
254   cations, and sulfate. Corresponding approximation could be adopted for each sub-domain
255   with the minimum numbers of equilibriums and unknown components. As listed in table
256   2, the numbers of sub-domains are 4, 5, 4, 2, 3, and 3 for the TEQM ISORRPIA-I,
257   ISORROPIA-II, MARS, RPMIRES, INCA, and EQSAM3, respectively.
258
259   The ways to account for the contribution of dust and sea salt to nitrate formation are also
260   different. Some models (EMAC, Oslo-CTM3, and Oslo-CTM2) include dust and/or sea
261   salt components in their TEQM models directly, while some models (EMEP, GISS-
262   OMA, GMI, and INCA) use an approach of first order loss rate outside their TEQMs to
263   account for the heterogeneous reactions of HNO_3 on the surface of dust and sea salt. For
264   the latter approach, the gamma rates and their RH dependence adopted by the models
265   differ as well.
266
267   Dry and wet deposition of NH_3, ammonium nitrate, and ammonium sulfate are treated
268   similarly to other gas and aerosol tracers in the models. It is worth pointing out that there
269   is a different consideration for Henry's law constant of NH_3 used by the models. Some
270   models modify it based on the pH value of cloud water while others do not. We will
271   discuss the impact of these two treatments on nitrate simulation in section 5.1.
272
273   We introduce only the major characteristics of thermodynamic equilibrium models since
274   this study aims for the evaluation and explanation of overall nitrate diversity among the
275   GCM/CTM models from all potential aspects. The detailed discussion of the models
276   chemical mechanism of gas phase reactions and the aerosol optical properties adopted by
277   the models is also beyond this work. Readers could refer to the references listed in Tables
278   1 and 2 for any further details.
279

Atmospheric
Chemistry
and Physics
Discussions

3. Observations

280
281 We use surface measurements from ground station networks and aircraft campaigns to
282 evaluate modeled surface concentrations, dry and wet depositions, and vertical
283 distributions of nitrate and related species (Table 3).
284

3.1 Surface measurements of concentrations and deposition rates

285
286 Ambient concentrations of sulfur and nitrogen species throughout the US and Canada
287 have been measured by the ground station network CASTNET (Clean Air Status and
288 Trends Network) (Figure 1). The measurements use a 3-stage filter pack with a controlled
289 flow rate. The measurements of CASTNET do not include NH_3. AMoN (Ammonia
290 Monitoring Network), measuring concentrations of ambient NH_3, has been deployed at
291 CASTNET sites starting from October 2007 using passive samplers. The corresponding
292 tracers' surface concentration measurements over Europe have been conducted by EMEP
293 (The European Monitoring and Evaluation Programme). The measured sites of all these
294 networks are located in rural areas or sensitive ecosystems, representing a larger region
295 by avoiding influences and contamination from local sources. Surface concentrations
296 over East Asia are inferred from the measurement of dry deposition by EANET (Acid
297 Deposition Monitoring Network in East Asia). This network provides acid deposition
298 from a regional monitoring network including 13 countries in East Asia using
299 standardized monitoring methods and analytical techniques.
300

301 CASTNET also provides dry deposition of sulfate and nitrogen species. Direct
302 measurements of dry deposition fluxes (D) are expensive so D is calculated as the
303 measured pollutant concentration (C) multiplied by the modeled dry deposition velocity
304 (V_d). V_d is either estimated by the Multi-Layer Model fed with measured hourly
305 meteorological data or derived from historical average V_d for sites with discontinued
306 meteorological parameters.
307

308 Direct measurements of wet deposition fluxes of sulfate, nitrate, and other ions have also
309 been performed by NADP/NTN (the National Atmospheric Deposition Program /
310 National Trends Network) across the contiguous US, Canada, Alaska, and the US Virgin
311 Islands and EANET over East Asia. Sites are predominantly located away from urban
312 areas and point sources of pollution. Each site has a precipitation chemistry collector and
313 gauge. Both networks can measure wet deposition for a continuous period (weekly for
314 NADP/NTN and daily for EANET), or every precipitation event if using an automated
315 collector (wet-only sampling).
316

317 Data is quality assured for all measurements. Measurements over North America use
318 automated screening techniques, semi-annual calibration results, site operator comments,
319 and manual data review. Quality assurance of EMEP is carried out on both the national
320 level and by the Chemical Co-ordinating Centre (CCC). The quality of EMEP
321 measurements is not equal at the national level (Schaap et al., 2002; 2004). Sites in
322 North, Western and Central Europe were generally well equipped and performing, while
323 sites in the rest of Europe suffered from inadequate sampling and calibrating methods due
324 to political and/or economical reasons. The quality of ammonia measurement is relatively
325 low since some laboratories experienced contamination problems (Williams et al., 1992).

Atmospheric
Chemistry
and Physics
Discussions

326   Although EANET adopts standardized monitoring methods and analytical techniques,
327   quality assurance is carried out on the national level.
328
329   **3.2 Aircraft measurements of vertical profiles**
330   Aircraft campaign measurements during the 2008 Arctic Research of the Composition of
331   the Troposphere from Aircraft and Satellites (ARCTAS) are used to evaluate tracer
332   vertical distribution simulated by the models (Bian et al., 2013; Jacob et al., 2010). Three
333   phases of the campaign, ranging from Northern Hemisphere mid-latitude industrial
334   region (ARCTAS-CARB, June 2008) to high latitude Arctic regions influenced by long-
335   rang pollution transport (ARCTAS-A, April 2008) and by local boreal biomass burning
336   (ARCTAS-B, July 2008), provide well encompassing environment observations. All
337   flights were conducted by the NASA DC-8 aircraft and the flight tracks of these three
338   phases are presented in Figure 2. An onboard HR-ToF-AMS instrument (Cubison et al.,
339   2011; DeCarlo et al, 2006) measured fine mode aerosol concentrations (PM1) along the
340   fight track including NO_3^-, NH_4^+, and SO_4^{2-} at STP conditions (1013mb and 273.15K) at a
341   sampling time interval of ~12 seconds. Accuracy estimate of 2-standard deviations, likely
342   conservative, is 34% for inorganics, dominated by the uncertainty in particle collection
343   efficiency due to particle bouncing (Huffman et al., 2005).
344
345   **4. Model intercomparison and evaluation**
346
347   **4.1 AeroCom model inter-comparisons of global distributions and budgets**
348   **4.1.1 NH_3 and NH_4^+**
349   Six models use HTAP2 anthropogenic emissions, two (GISS-MATRIX and GISS-OMA)
350   use CMIP5 emissions, and one (INCA) uses ECLIPSE emissions. Table 4b shows that
351   eight models have the annual NH_3 emission values within 5% of the value from the
352   AeroCom experiment recommended emission inventories, but INCA is 11% higher. The
353   similar emission distributions ensure that the examined inter-model diversities are truly
354   caused by the differences in physicochemical processes among the models. The
355   normalized root-mean-square deviation (NRMSD) of NH_3 global burden among models
356   is 1.17 and 0.33 with and without EMAC included. This drastic change in global burden
357   NRMSD by EMAC is caused by its special treatment of wet deposition. In fact, the
358   removal of trace gases and aerosol particles by clouds and precipitation in EMAC is not
359   calculated based on empirically determined, fixed scavenging coefficients, but rather by
360   solving a system of coupled ordinary differential equations, explicitly describing the
361   processes involved (Tost et al., 2006). This method resolves feedback mechanisms
362   between the multi-phase chemistry and transport processes involved. The liquid phase
363   reaction set used converts all the scavenged NH3 (or HNO3) into NH_4^+ (or NO_3^-) in the
364   liquid phase so that at the end everything that is deposited is the total NH_4^+ and NH3.
365
366   Atmospheric NH_4^+ is produced entirely by NH_3 chemical transformation. The models
367   simulate NH_4^+ much closer in chemical production (difference less than a factor of 2) than
368   in lifetime (difference up to a factor of 5.2), indicating removing rates are a key factor in
369   controlling the global burden of NH_4^+. For example, CHASER has a much longer lifetime
370   of NH_4^+ (i.e. 9.8 days versus 4.3 days in average), which indicates a slow deposition

Atmospheric
Chemistry
and Physics
Discussions
Open Access
EGU

371   removal of NH_4^+ from the atmosphere. Consequently, CHASER simulates a much higher
372   atmospheric NH_4^+ burden than other models.

373

374   **4.1.2 HNO_3 and NO_3^-**
375   HNO_3, an important nitrate precursor, differs by up to a factor of 9 in its global
376   tropospheric burden among the models (Table 4c). All models simulated HNO_3 based on
377   a full gas phase O_3-HO_x-NO_x chemistry and coupled it with aerosol chemistry. This
378   HNO_3 diversity will naturally be propagated into the NO_3^- simulation. However, further
379   discussion of the detailed consideration of full gas-aerosol chemistry for HNO_3 diversity
380   among the models is beyond the scope of this study.

381

382   The resultant aerosol product (i.e., NO_3^-) does not entirely follow its precursor (i.e.,
383   HNO_3) in terms of global burden: EMEP has very low HNO_3 but high NO_3^-, two GISS
384   models (MATRIX and OMA) simulate high HNO_3 but low NO_3^-, while OsloCTM3 has
385   an average HNO_3 but more than triple high NO_3^- than average (Tables 4a and 4c).
386   Furthermore, the difference in NO_3^- global burden (up to a factor of 13) is larger than that
387   of HNO_3. Differences in chemical mechanisms of NO_3^- production could be a potential
388   explanation along with the difference in HNO_3 precursor. Unfortunately, only GMI and
389   INCA provide a detailed NO_3^- chemistry budget analysis. Nevertheless, we can infer that
390   the total chemical production of NO_3^- must be very low (~ 10Tg) in the two GISS models
391   while very high (> 100 Tg) in OsloCTM2 and OsloCTM3 based on the reported total
392   NO_3^- loss. Combining this information with the HNO_3 global tropospheric burden (Table
393   4c), we can further infer that the chemical conversion from HNO_3 to NO_3^- must be lowest
394   in the two GISS models while highest in the two Oslo models. Several factors could
395   influence this conversion, such as the availability of alkaline species of mineral dust and
396   sea-salt particles and the physicochemical mechanism of nitrate formation on dust and
397   sea-salt, availability of NH_3 after combining with SO_4^{2-}, and the atmospheric
398   meteorological fields of temperature and relative humidity. More discussions are given in
399   sections 5.2 and 5.3.

400

401   Atmospheric lifetime of NO_3^- differs up to a factor of 4, from about 2 days in GMI and
402   OsloCTM2 to larger than 7 days in GISS-OMA and GISS-MATRIX. The slower removal
403   processes in the two GISS models compensate the low chemical production and help to
404   maintain their NO_3^- atmospheric burden (Figure 3 and Table 4a).

405

406   **4.2 Model-observation comparisons**

407

408   **4.2.1 Comparisons of surface concentrations over North America, Europe, and East**
409   **Asia**
410   Understanding diversity among model simulations and potential physiochemical
411   processes behind the difference is important but not sufficient. The information has to be
412   combined with the knowledge of model performance obtained directly from comparisons,
413   particularly down to processes level, against various measurements to gain a direction of
414   any improvement. Figures 4a-c show a model-observation comparison for surface
415   mass/volume mixing ratios of NO_3^-, NH_4^+, NH_3, HNO_3, and SO_4^{2-} over North America
416   (CastNET), Europe (EMEP), and East Asia (EANET). Each point represents a monthly

Atmospheric
Chemistry
and Physics
Discussions

417 mean concentration at one observational site. Generally, the agreement between model
418 and observation is better for aerosol components than for gas tracers (i.e. the precursor
419 species NH_3 and HNO_3) over all three regions. All models underestimate NH_3 surface
420 volume mixing ratio with a ratio of model to observation down to 0.14, while most
421 models overestimate surface HNO_3 volume mixing ratio with a ratio up to 3.9 over North
422 America. The worse performances of NH_3 against observations may be also associated to
423 their relatively lower measurement accuracy, i.e. easier to be contaminated during
424 measurement (Williams et al., 1992). Among aerosol simulations, model performance is
425 very similar for NH_4^+ and SO_4^{2-}, while slightly worse for NO_3^- that is dispersed further
426 away from the 1:1 line, particularly at low NO_3^- values. The NO_3^- simulation over East
427 Asia is worst with the average normalized root mean square to be 1.3 and 1.8 higher than
428 that over North America and Europe, respectively.
429
430 **4.2.2 Comparisons of vertical profiles with aircraft measurements during the**
431 **ARCTAS field campaign**
432 Evaluation of model performance presented in 4.2.1 for the surface concentrations in the
433 source regions is highly dependent on the accuracy of the emission inventory. On the
434 other hand, evaluation using aircraft measurements, particularly over remote regions,
435 provides further examination of models' physicochemical evolution during transport.
436 Here we use data from three phases of the ARCTAS aircraft campaign (section 3), and
437 the results are shown in Figure 5. All model results of NO_3^-, NH_4^+, and SO_4^{2-} are sampled
438 along flight track and averaged regionally within 1km vertically for each campaign phase
439 before comparing with the corresponding aircraft measurements. Note that only EMAC,
440 EMEP and GMI report daily 3D global tracer concentrations, while the others report
441 monthly only. Note also that only EMEP and GMI adopt daily biomass burning emission
442 while the others use monthly emission. To verify the representativeness of monthly mean
443 concentration in capturing the main features exhibited in model-observation comparisons,
444 daily and monthly concentrations of the three models are used in the same spatial
445 sampling to compare with the measurements (see the green lines for daily and red for
446 monthly in the figure). The comparison keeps its main features as shown when using both
447 daily and monthly model data.
448
449 During ARCTAS-A, which was conducted in April 2008 and was based in Fairbanks,
450 Alaska, none of the models captures the long-range transport of aerosols primarily from
451 Asia, which enter Polar Regions at altitudes between 2-7 km (Fig. 3 in Bian et al., 2013).
452 Except CHASER and EMAC, all models also report a significant underestimation of
453 NH_4^+ and SO_4^{2-} in boundary layer. A previous assessment of pollution transport to the
454 Arctic indicated that aerosol wet removal plays an important role in the uncertainty of
455 Arctic aerosols (Shindell et al., 2008). Another potential reason is that some large fire
456 activities in Siberia during April 2008 (Jacob et al., 2010) may be missed in the GFED3
457 emission inventory. The underestimation of SO_4^{2-} may help bring up NO_3^- production,
458 particularly at high altitudes. During ARCTAS-CARB, which was conducted in June
459 2008 based in Palmdale, California, agreement between model and measurements is
460 much improved. Almost all models show a rapid vertical decease from surface to free
461 troposphere, which is consistent with the measurements of SO_4^{2-} and NH_4^+, but not NO_3^-.
462 The observation shows a maximum of NO_3^- at about 1.5 km, which is not represented by

Atmospheric
Chemistry
and Physics
Discussions

463   any of the models. During ARCTAS-B, which was conducted in July 2008 and was based
464   in Cold Lake, Canada, when there were frequent local wild fires, model performances are
465   mixed. In general, most models underestimate concentrations of NO_3^-, NH_4^+ and
466   SO_4^{2-} below 4 km. CHASER model is special in that it overestimates SO_4^{2-} significantly.
467   This may be contributed to high (near surface) to comparable (free troposphere) model
468   simulation of NH_4^+ but an underestimation of NO_3^-. Different from other models, the
469   INCA model shows an enhancement of pollutants in the upper troposphere with
470   concentrations much higher (more than 5 times) than observations. This behavior may be
471   derived from a much vigorous vertical uplifting to the upper troposphere as revealed from
472   Fig. 3a-3b combined with a low NH_3 Henry's law constant used by INCA, see discussion
473   in section 5.2.
474
475   Note that all measurements and model data we discussed above are for fine mode
476   aerosols. Total NO_3^- (orange line using monthly model output) is also shown in the figure
477   to reveal whether a changing of partitioning of fine and coarse mode NO_3^- could improve
478   the model-observation comparison. It seems that the new version of OsloCTM3 may put
479   too much of NO_3^- in coarse mode.
480
481   **4.3 Model-observation comparison for dry and wet deposition**
482
483   **4.3.1 Dry deposition**
484   The budget analyses in section 4.1 concluded that dry and/or wet depositions are most
485   likely the main processes driving the diversity in the model simulations. Thus, further
486   evaluation of deposition processes is needed to identify any potential problematic model.
487
488   The dry depositions of NO_3^-, NH_4^+, HNO_3, and SO_4^{2-} simulated by the models are
489   compared against CASTNET measurements over North America (Figure 6). Generally,
490   the overestimation of surface HNO_3 concentrations (Figure 3a) results in the higher dry
491   depositions of HNO_3, but this is not the case for NO_3^-. Meanwhile, most of the models
492   give a better dry deposition simulation for aerosol SO_4^{2-} and NH_4^+ than for aerosol NO_3^-,
493   except CHASER. Specifically, GISS-OMA and GISS-MATRIX have wide spread dry
494   NO_3^- deposition at any given measurement value. In other words, the two models
495   underestimate NO_3^- dry deposition significantly at many observational stations, which
496   does not occur in the other models. This low dry deposition simulation may occur outside
497   North America as well because the global dry depositions of the two models are lower
498   than others (Table 4a). OsloCTM2 overestimates NO_3^- dry deposition significantly, which
499   is probably linked to its larger coarse fraction of the nitrate aerosol (see discussion in
500   section 5.3). OsloCTM3 improved its dry deposition scheme although the model still
501   overestimates the dry deposition. We will discuss the OsloCTM2 NO_3^- simulation over
502   North America by combining the model's wet deposition in the next section. NH_4^+ dry
503   deposition is low in GMI but very high in CHASER. This performance is also extended
504   globally as summarized in Table 4b.
505
506   **4.3.2 Wet deposition**
507   The wet deposition simulations from the nine models are compared with surface
508   measurement over North America (Figure 7a) and East Asia (Figure 7b) for oxidized

Atmospheric
Chemistry
and Physics
Discussions

509   NO_3^- (i.e. total NO_3^- and HNO_3), total NH_4^+ and NH_3 (tNH_4^+), and SO_4^{2-}. All models tend
510   to underestimate the wet deposition of tNH_4^+ and SO_4^{2-} over the two regions. Models
511   EMAC, GMI, OsloCTM2 and OsloCTM3 have relatively high wet removal for oxidized
512   NO_3^-, while EMEP removes much less than others over North America. All models' wet
513   deposition of oxidized NO_3^- is biased low over East Asia. As we discussed above,
514   OsloCTM2 and OsloCTM3 have very high dry NO_3^- depositions (Figure 6) compared
515   with CASTNET observations. The overall high dry and wet NO_3^- depositions along with
516   high atmospheric concentrations (Figure 4a) indicate that the chemical formation of
517   NO_3^- in the two models must be also high. This performance might be also true on global
518   scale since the inferred chemical productions of NO_3^- in the two models are the highest
519   (Table 4a). CHASER has the lowest tNH_4^+ wet deposition. This may result in a very high
520   NH_4^+ dry deposition (Figure 6) and concentration (Figures 4a-c, 5) compared with
521   observations and other models. Overall, wet deposition seems to be the dominant process
522   in determining the diversity in NH_3 and NH_4^+ lifetime (Table 4b).

524   Note that we use the traditional approach of comparing models' grid box mean values
525   with observations, which does not take into account the impact of the models' horizontal
526   resolutions in their representation of observations (Schutgens et al., 2016). Since majority
527   models (except EMEP) have horizontal resolutions around 2-3 degrees, the models grid
528   box means tend to smooth out extreme (i.e. very low or high) observations. Reflecting on
529   the scattering plots of model (y-axis) and observation (x-axis) is that the slopes of fitting
530   lines are generally less than 1 (Figures 4a-d, 6, 7a-b).

532   **5. Discussion of major uncertainties in nitrate formation**
533   Large uncertainties of nitrate studies result from the complexity of the simulations which
534   must consider a comprehensive NO_x-NMHC-O_3-NH_3 chemistry and a thermodynamic
535   equilibrium model (TEQM) to partition semi-volatile ammonium nitrate between the gas
536   and aerosol phases. Nitrate aerosol concentrations depend on temperature, relative
537   humidity (RH), and concentrations of HNO_3, NH_3, NH_4^+, SO_4^{2-}, Cl^-, Na^+, Ca^{2+}, K^+,
538   Mg^{2+}, organic acids, among others. A further complicating factor is that the equilibrium
539   for the coarse mode is somewhat questionable (Feng and Penner, 2007). In addition, wet
540   removal of NH_3 is very sensitive to the correction of pH in cloud water. We will discuss
541   some of these uncertainties below.

543   **5.1 pH-dependent NH_3 wet deposition**
544   Gas tracer NH_3, a precursor of ammonium aerosol, experiences atmospheric wet
545   deposition and its deposition rate is typically calculated using Henry's Law. Henry's law
546   constant (H) of gases in water is usually given at 298 K (indicated by Θ in superscript)
547   and can be adjusted by temperature (T).

$$H(T) = H^{\Theta} * \exp\left(-\frac{\Delta H_{sol}}{R}\left(\frac{1}{T} - \frac{1}{T^{\Theta}}\right)\right) \qquad (1)$$

548   Here ΔH_{sol} is the enthalpy of dissolution and R is the gas constant.

550   For some acidic/basic gases, including NH_3, Henry's law constant is also a function of
551   pH in cloud water (a.k.a effective Henry's law constant $H^{\Theta*}$). As explained in the
552   Appendix, the $H^{\Theta*}$ is inferred from H^{Θ} with a correction of pH (pH = $-\log_{10}[H^+]$) as

Atmospheric
Chemistry
and Physics
Discussions

$$H^{\Theta*} = H^{\Theta} \frac{K_{al}[H^+]}{K_w} \qquad\qquad (5)$$

553   Here, $K_{al} \approx 1.8 \times 10^{-5}$ and $K_w = 1.0 \times 10^{-14}$ at 298 K in pure water (see Appendix). However,
554   not every model accounts for pH adjustment (i.e. the reaction of equation 2 in Appendix)
555   for NH_3 dissolution. More accurately, the EMAC model implicitly calculates the
556   effective Henry's law constant by solving a set of partial differential equations, which
557   includes not only the gas-liquid phase equilibria, but also the reactions in the liquid phase
558   (i.e. dissociation or acid-base equilibria, Redox reactions and photolysis reactions in the
559   liquid phase, see Tost et al.(2006)). Therefore, the gas-liquid phase equilibrium is
560   explicitly calculated based on the chemical mechanism used in the liquid phase. As listed
561   in Table 5, the rest of the models are generally divided into two groups based on their
562   effective Henry's law constant: (1) INCA, GISS-OMA and GISS-MATRIX has $H^{\Theta*} \leq$
563   100 (L-theta without pH correction) and (2) CHASER, GMI, OsloCTM2 and Oslo-
564   CTM3 has $H^{\Theta*} > 10^{+5}$ (H-theta with pH correction). The NH_3's $H^{\Theta*}$ adopted by the
565   models varies dramatically, up to an order of 6 in magnitude among all the models and a
566   factor of 10 just for the models in H-theta group (Table 5). The latter is corresponding to
567   a correction for pH ranging from 4.5 (Oslo-CTM2) to 5.5 (CHASER).
568
569   To examine how sensitive of NH_3, NH_4^+ and NO_3^- simulations in response to the
570   magnitude of NH_3's $H^{\Theta*}$, we performed a sensitivity experiment, named TWET, in the
571   GMI model in which there was no pH adjustment for NH_3 Henry's law constant (i.e.
572   $H^{\Theta*}$=61 instead of 1.05e+6, see table 6). The resultant annual budgets of dry/wet
573   deposition, chemistry production and loss, and atmospheric loading of NH_3,
574   NH_4^+ and NO_3^- are summarized in Table 7, the tracers' vertical zonal mean distributions
575   are shown in Figure 8, and the comparisons with the ARCTAS measurements for
576   NH_4^+ and NO_3^- are shown in Figure 9. For convenient comparison, the GMI baseline
577   results are given in the table and figures as well. There is a dramatic decrease (from 17.5
578   to 1.1 Tg) in NH_3 wet deposition when using pure water NH_3 Henry's law constant.
579   Consequently, NH_3 will remain in the atmosphere (i.e. ~ 8 times more atmospheric NH_3)
580   to produce ~1.6 times more NH_4^+ chemically. This, in turn, greatly increases atmospheric
581   NO_3^- to 0.97 Tg from 0.26 Tg reported in baseline simulation. A large portion of the
582   increased NH_3, NH_4^+ and NO_3^- resides in the upper troposphere and close to the
583   tropopause region, while the changes of the tracers in the lower troposphere are relatively
584   small, as shown in Figure 8. These accumulations at high altitudes are far above (i.e. ~ 50
585   times for NH_4^+ and NO_3^-) the ARCTAS observed tracer amounts as shown in Figure 9.
586   The TWET experiment might be an explanation of NH_4^+ and NO_3^- accumulations near the
587   tropopause region (Figure 3a-b) in the INCA model whose NH_3 Henry's law constant H^{Θ}
588   is 74 without pH correction (i.e. a L-theta model, table 5). However, it is puzzling that the
589   NH_3 simulations by GISS-MATRIX and GISS-OMA, those are the models with L-theta,
590   are closer to the simulations of the models with H-theta, i.e. no NH_4^+ and NO_3^-
591   accumulation near the tropopause and comparable removal of NH_4^+ (Figure 3a-b and
592   Table 4b).
593
594   **5.2 Contribution of dust and sea salt on nitrate formation**
595   In the presence of acidic accumulation-mode sulfuric acid containing aerosols, HNO_3,
596   NO_3 radicals, and N_2O_5 will deposit on larger alkaline mineral or salt particles (Dentener

597   et al., 1996; Gard et al., 1998; Hauglustaine 2014; Karydis et al., 2016; Murphy and
598   Thomson 1997; Paulot et al., 2016). Considerable evidence shows that the majority of
599   atmospheric nitrate is formed via reactions associated with dust and sea salt (Allen et al.
600   2015; Itahashi et al., 2016; Karydis et al., 2016). Coarse mode nitrate overwhelmingly
601   dominates over remote oceanic regions (Itahashi et al., 2016). Over wide land regions,
602   nitrate also quite often exists in the form of supermicron NO_3^- balanced by the presence
603   of mineral cations arising from transport of crustal dust and sea spray aerosol (Allen et
604   al.,2015; Lefer and Talbot; 2001).

606   Investigation of nitrate interactions with mineral dust and sea salt depends on the
607   simulation approach adopted in a model. The traditional equilibrium approach to partition
608   semi-volatile HNO_3 between the gas and aerosol phases is no longer possible since the
609   time to reach equilibrium on coarse mode particles (several hours to days) is typically
610   much longer than the chemical time step used in a global model (less than 1 hour) (John
611   et al., 1989; Myhre et al., 2006). Meng and Seinfeld (1996) found that on longer time
612   scales, when NH_3/HNO_3 started to condense on larger aerosols, their gas phase
613   concentrations decreased so that some of the condensed matter can be driven back to the
614   gas phase from the small semi-volatile aerosols. A fix to a non-equilibrium state would
615   be to implement a kinetic formulation for the particles that have a long equilibrium time
616   scale (Feng and Penner, 2007; Karydis et al., 2010). However, implementing explicit
617   kinetics in a global model would be computationally expensive and, hence, is not feasible
618   for long-term climate simulations. Several approximations, therefore, have been
619   developed to compromise accuracy and efficiency.

621   Four such approximations are adopted by the nine models participating in this study: 1)
622   using equilibrium calculations for fine mode particles only while neglecting nitrate
623   formation on coarse mode particles (CHASER and GISS-MATRIX); 2) combining
624   equilibrium calculation for a solution of SO_4^{2-}-NO_3^--NH_4^+-H_2O and heterogeneous
625   reaction calculation for nitrogen uptake on dust and sea-salt using a first-order loss rate
626   (EMEP, GMI, GISS-OMA and INCA); 3) running equilibrium model including NH_3,
627   dust and sea salt repeatedly for aerosol sizes from fine mode to coarse mode (Oslo-CTM2
628   and Oslo-CTM3); and 4) using only the fraction of the gas that can kinetically condense
629   within the time step of the model in the equilibrium calculations for each aerosol size
630   mode (EMAC).

632   Nitrate is formed primarily on dust and sea salt by GMI (88%) and INCA (82%) (see
633   Table 4a). INCA further separates the formation as 45% on dust and 37% on sea-salt. The
634   above-mentioned approach 1 is problematic due to absence of coarse mode nitrate, an
635   important portion of nitrate, which results in relatively low nitrate burdens for CHASER
636   and GISS-MATRIX. Unfortunately, the other models are missing a detailed nitrate
637   chemistry budget report. A potential impact of dust and sea-salt on nitrate formation,
638   nevertheless, can be inferred from the approach adopted by a model. For example,
639   OsloCTM2 and OsloCTM3 adopt approach 3. Although the model allows fine mode
640   particles to reach equilibrium first, the subsequent equilibrium calculation for coarse
641   mode particles may still produce coarse mode nitrate too quickly, see discussion of the
642   ratio of coarse model nitrate in the next subsection. To avoid such overestimations on the

Atmospheric
Chemistry
and Physics
Discussions
Open Access
EGU

643   production of coarse mode nitrate, EMAC allows only a fraction of HNO_3 to partition in
644   the aerosol phase by assuming diffusion limited condensation (Pringle et al., 2010).
645
646   To further understand the role of homogeneous and heterogeneous chemical reaction
647   processes in nitrate formation, we conducted two more sensitivity experiments,
648   TnoCNH3 and TnoCHET, with the GMI model (Table 6). Experiment TnoCNH3 turned
649   off chemical conversion of NH_3 to NH_4^+ in the GMI thermodynamic equilibrium model,
650   while experiment TnoCHET excluded the nitrate formation via heterogeneous reaction of
651   gas HNO_3 on the particles of dust and sea salt. The budget report, vertical zonal mean
652   distribution and model-observation comparison of NH_3, NH_4^+ and NO_3^- are given in Table
653   7 and Figures 8-9, respectively. It is not surprising that experiment TnoCNH3 gives a
654   higher atmospheric NH_3 burden (0.32 Tg) compared with baseline (0.11 Tg) with little
655   NH_4^+ left (from its initial field). The interesting thing is that the formed NO_3^- has only
656   slightly decreased compared with baseline (from 0.26 to 0.20 Tg), confirming the
657   importance of NO_3^- formation via dust and sea salt. For experiment TnoCHET, the
658   simulations of NH_3 and NH_4^+ stay the same but the formed NO_3^- is decreased dramatically
659   (from 0.26 to 0.10), indicating that NO_3^- formation via NH_3 chemistry alone in the GMI
660   model is relatively small. The chemical production of NO_3^- is about 6 times larger in
661   TnoCNH3 (via dust and sea salt) than in TnoCHET (via NH_3). However, the NO_3^-
662   produced via NH_3 chemistry (TnoCHET) is non-negligible over remote regions impacted
663   by long-range transport, as shown in the analysis of April Alaska observations in Figure
664   9.
665
666   **5.3 Nitrate size distribution**
667   Unlike sulfate aerosol, a noticeable fraction of nitrate aerosol is in the coarse mode.
668   Having an accurate aerosol size distribution is critical in climate forcing estimations,
669   since large size particles have a relatively small optical cross section at a given aerosol
670   mass loading and the nitrate material coating on dust particles has almost no direct impact
671   on the dust optics, although the greatly impact dust lifetime (Bauer et al., 2007). Given
672   that the deposition velocity of a coarse particle is greater than that of a fine particle, an
673   accurate size distribution is also necessary to estimate deposition of particulate nitrates
674   (Yeatman et al., 2001; Sadanaga et al., 2008). This estimation is particularly important
675   over oceans where coarse mode nitrate dominates (Itahashi et al., 2016) and nitrogen
676   supply is often in deficit (Hansell and Follows, 2008).
677
678   As we have discussed in section 5.2, nitrate size distribution varies with the approaches
679   adopted for nitrate formation on coarse mode aerosols (i.e. dust and sea salt). Figure 10
680   gives the burdens of nitrate in fine mode and coarse mode portions and the ratio between
681   coarse mode and total (f_c) for the eight discussed models. The ratio is ranging from 0
682   (CHASER and GISS-OMA), ~50% (EMAC, GMI and INCA), ~80% (EMEP and
683   OsloCTM2), and 97% (OsloCTM3). The two OsloCTMs give the highest f_c partially
684   because they run TEQM model for coarse model particles.
685
686   A wide range of f_c, from 0 to > 90%, has been reported previously by model
687   simulations (Adams et al., 2001; Bauer et al., 2007; Jacobson 2001), while the range is
688   narrowed down to 40-60% for the model studies using the approach that solves dynamic

Atmospheric
Chemistry
and Physics
Discussions

689   mass transfer equation for coarse mode particles (Feng and Penner, 2007; Xu and Penner,
690   2012).
691
692   It is worth pointing out that aerosol microphysics modify aerosol size as well. For
693   example, a process like coagulation would also allow NO_3^- to mix with other particles and
694   enter coarse mode aerosol. New particle formation/nucleation would add $NH_3/NH_4^+/NO_3^-$
695   into the ultra fine mode. Except EMAC and GISS-MATRIX, majority models involved in
696   this study are bulk aerosol models that do not account for aerosol microphysics.
697
698   It is challenging to verify the nitrate size distribution globally due to the limited
699   measurements on time and space. Measurements over regional and station sites indicated
700   that the ratio of f_c could be very high and vary seasonally over oceanic sites. For
701   example, annual mean f_c during 2002-2004 from the Fukue supersite observatory is
702   about 72% with a seasonal variation of 60–80% in winter and of around 80% in summer
703   (Itahashi et al., 2016).
704
705   However, the ratio could be varied dramatically over land or the areas affected by land
706   pollution. For example, observations of fine and coarse particulate nitrate at several rural
707   locations in the United States indicated that nitrate was predominantly in submicron
708   ammonium nitrate particles during the Bondville and San Gorgonio (April) campaigns, in
709   coarse mode nitrate particles at Grand Canyon (May) and Great Smoky Mountains
710   (July/August), and both fine and coarse mode nitrate during the studies at Brigantine and
711   San Gorgonio (July) (Lee et al., 2008). Allen et al. (2015) examined aerosol composition
712   data collected during the summer 2013 SOAS and concluded that inorganic nitrate in the
713   southeastern United States likely exists in the form of supermicron NO_3^-, balanced by the
714   presence of mineral cations arising from the transport of crustal dust and sea spray
715   aerosol. The measurements over Harvard Forest, a rural site in central Massachusetts,
716   supported that the majority of nitrate mass was associated with water-soluble
717   supermicron soil-derived Ca^{2+} in an acidic environment (Lefer and Talbot, 2001).
718   Measurements of coarse-mode aerosol nitrate and ammonium at two polluted coastal
719   sites, Weybourne, England and Mace Head, Ireland, during polluted flow when the air
720   had passed over strong source regions of the UK and northern Europe, showed 40–60%
721   of the nitrate was found in particles with diameter >1 μm, but under clean marine
722   conditions almost 100% conversion was seen (Yeatman et al., 2001).
723
724   **6. Conclusions**
725
726   We present the AeroCom phase III nitrate study by assessing aerosol simulations of
727   nitrate and ammonium and their precursors with nine global models. Five of the models
728   couple the chemical calculation online with meteorological simulation, and four use
729   archived meteorological fields driving chemistry. To focus on chemical-physical
730   processes behind the diversity of nitrate simulation, all participating models are
731   encouraged to use HTAP2 emission inventory. The simulated aerosols of nitrate and
732   ammonium and their precursors are compared among the models and evaluated against
733   various measurements including surface concentrations and dry/wet depositions from
734   surface measurements, and vertical distributions from aircraft measurements.

Atmospheric
Chemistry
and Physics
Discussions

735
736 All models capture the main features of the distribution of nitrate and ammonium: large
737 surface and column amounts over China, South Asia, Europe, and U.S. These regions are
738 typically densely populated with large NH_3 and NO_x emissions. Many models also show
739 enhanced nitrate and ammonium over the Middle East and continents over the Southern
740 Hemisphere. The former undergoes huge dust pollution and the latter experiences fires
741 that emit both NH_3 and NO_x.
742
743 The diversity of nitrate and ammonium simulations among the models is large: the ratio
744 of the maximum to minimum quantities among the nine models is 13.4 and 4.4 for model
745 simulated global mass burdens of nitrate and ammonium, respectively, and 3.9 and 5.2
746 for the corresponding lifetimes. These values are also larger than those of sulfate: 4.0 for
747 global burden and 3.0 for lifetime.
748
749 The agreement between models and observations is better for aerosol components than
750 for gas tracers. All models underestimate NH_3 surface mass concentrations but most
751 models overestimate surface HNO_3 concentrations over North America and East Asia.
752 Performance of NH_3 is the worst: this could partially be associated to its relatively lower
753 measurement accuracy, i.e. a loss of ammonia possibly on the filters designed to collect
754 NH_3 (Williams et al., 1992). Among aerosol simulations, model performance based on
755 evaluation of surface mixing ratio and dry/wet depositions is very similar for NH_4^+ and
756 SO_4^{2-}, while slightly worse for NO_3^-. Models severely underestimate the aerosol
757 concentrations with only a few exceptions when compared with aircraft measurements
758 and this problem is worse over regions impacted by long-range transport than those
759 closer to sources.
760
761 There are many intrinsic reasons for a larger diversity in nitrate simulations among
762 models. Nitrate is involved in much more complicated chemistry: the chemical
763 mechanism needs to handle a multiphase multicomponent solution system. The system
764 sometimes cannot even be solved using the thermodynamic equilibrium approach when
765 coarse mode dust and sea salt particles present. A reasonable nitrate simulation also
766 depends on good simulations of various precursors, such as NH_3, HNO_3, dust and sea
767 salt, although models account for impact of dust and sea salt very differently. Even an
768 accurate simulation of SO_4^{2-} is a prerequisite because SO_4^{2-} surpasses NO_3^- at reacting
769 with NH_4^+.
770
771 The models' intercomparison and model-observation comparison revealed at least two
772 critical issues in nitrate simulation that demand further exploration: NH_3 wet deposition
773 and relative contribution to NO_3^- formation via NH_3 and dust/sea salt. The nine
774 participating models adopt very different effective Henry's law constants for NH_3, with
775 one group having a value equal or less than 100 (in pure water) and the other larger than
776 1.e+05 (with pH correction). Sensitivity studies using the GMI model indicated that
777 without pH correction, NH_3 wet deposition decreases massively (from 17.5 to 1.1 Tg),
778 which prolongs atmospheric NH_3 lifetime (from 0.67 to 5.2 days) and enhances its
779 atmospheric burden (from 0.11 to 0.85 Tg), and thus the atmospheric burden of NH_4^+
780 (from 0.17 to 0.48 Tg) and NO_3^- (from 0.26 to 0.97 Tg) as well. These enhanced tracers

Atmospheric
Chemistry
and Physics
Discussions

Open Access

781   tend to accumulate in the upper troposphere and close to the tropopause, and are too high
782   when compared with aircraft measurements.
783
784   All the models use thermodynamic equilibrium to solve the chemical process of
785   NH_3/NH_4^+ to NO_3^- formation in fine model aerosols. However, the models adopt very
786   different ways in accounting for the contribution of these reactions on the surface of dust
787   and sea salt particles: some account for both dust and sea salt, some account for only dust
788   or only sea salt, and two models even do not account for any heterogeneous reactions.
789   The methodologies that take dust and sea salt into account are also very different, i.e.
790   together with NH_4^+ using thermodynamic equilibrium model or simply adopting a first
791   order loss rate on dust and sea salt surfaces. The chemical budget reported by GMI and
792   INCA indicates that the majority (>80%) of global NO_3^- formation is via reaction on dust
793   and sea salt. Two sensitivity experiments using the GMI model by tagging the NO_3^-
794   formation from either NH_3/NH_4^+ chemistry or heterogeneous reactions on dust and sea
795   salt confirm the critical importance of the latter process, and indicate that the former
796   process is relatively important in remote regions. The importance of NO_3^- formation on
797   dust and sea salt lies also in its determination on nitrate particle size distribution, so that
798   has an implication in air quality and climate studies as well.
799
800   Our work presents a first effort to assess nitrate simulation from chemical and physical
801   processes. A companion study is proposed by AeroCom III nitrate activity to investigate
802   how sensitive is nitrate formation in response to the possible future changes of emission
803   and meteorological fields. These perturbation fields include increasing NH_3 emission,
804   decreasing NOx, SOx and dust emissions, and increasing atmospheric temperature and
805   relative humidity. Based on the findings of this work, modelers should pay particular
806   attention to incorporating dust and sea salt and treating NH_3 wet deposition to improve
807   nitrate simulation. Further evaluation using satellite measurements, such as NH_3 products
808   from IASI and TES, is desired and will be conducted. Such evaluation requires global 3-
809   dimensional high frequency model data. Potential future study also includes estimation of
810   nitrate forcing for climate change.
811
812   **Appendix**
813   For some acidic/basic gases, including NH_3, Henry's law constant is also a function of
814   pH in water (a.k.a effective Henry's law constant). This is because not only does the
815   aqueous chemistry reaction $NH_3 + H_2O$ (equation 1) reach equilibrium within a chemical
816   time step but its product $NH_3 \cdot H_2O$ (equation 2) does as well.

$$NH_3 + H_2O \Leftrightarrow NH_3 \cdot H_2O \qquad (1)$$
$$NH_3 \cdot H_2O \Leftrightarrow NH_4^+ + OH^- \qquad (2)$$

817   Here, NH_4^+ is the ammonium ion and OH^- is the hydroxide ion. The total dissolved
818   ammonia $[NH_3^T]$ is given by

$$
\begin{aligned}
[NH_3^T] &= [NH_3 \cdot H_2O] + [NH_4^+] \\
&= p_{NH3} H^\Theta \left(1 + \frac{K_{al}[\text{H}^+]}{K_w} \right) \\
&\approx p_{NH3} \left(H^\Theta \frac{K_{al}[\text{H}^+]}{K_w} \right) \qquad (3)
\end{aligned}
$$

Atmospheric
Chemistry
and Physics
Discussions

819   Here, p_{NH3} is the partial pressure of NH_3, $K_{al} = [NH_4^+][OH^-] / [NH_3 \bullet H_2O] \approx 1.8 \times 10^{-5}$, and

820   $K_w = 1.0 \times 10^{-14}$ at 298 K in pure water. So the effective Henry's law constant $H^{\Theta*}$ is

821   inferred from H^{Θ} with a correction of pH (pH = $-\log_{10}[H^+]$) as

$$H^{\Theta*} = H^{\Theta} \frac{K_{al}[H^+]}{K_w} \qquad\qquad (4)$$

822

823   **References:**

824   Allen1,H. M., D. C. Draper1, B. R. Ayres, A. Ault, A. Bondy, S. Takahama, R. L. Modini, K. Baumann, E.
825   Edgerton, C. Knote, A. Laskin, B. Wang, and J. L. Fry, Influence of crustal dust and sea spray
826   supermicron particle concentrations and acidity on inorganic NO3 aerosol during the 2013 Southern
827   Oxidant and Aerosol Study, Atmos. Chem. Phys., 15, 10669–10685, 2015, www.atmos-chem-
828   phys.net/15/10669/2015/, doi:10.5194/acp-15-10669-2015.
829   Bauer, S. E., Balkanski, Y., Schulz, M., Hauglustaine, D. A., and Dentener, F.: Global modeling of
830   heterogeneous chemistry on mineral aerosol surfaces: Influence on tropospheric ozone chemistry and
831   comparison to observations, J. Geophys. Res.-Atmos., 109, D02304, doi:10.1029/2003jd003868, 2004.
832   Bauer, S.E., and D. Koch, 2005: Impact of heterogeneous sulfate formation at mineral dust surfaces on
833   aerosol loads and radiative forcing in the Goddard Institute for Space Studies general circulation
834   model. J. Geophys. Res., 110, D17202, doi:10.1029/2005JD005870.
835   Bauer, S. E., Koch, D., Unger, N., Metzger, S. M., Shindell, D. T., and Streets, D. G.: Nitrate aerosols
836   today and in 2030: a global simulation including aerosols and tropospheric ozone, Atmos. Chem.
837   Phys., 7, 5043–5059, doi:10.5194/acp-7-5043-2007, 2007.
838   Bauer, S.E., D. Wright, D. Koch, E.R. Lewis, R. McGraw, L.-S. Chang, S.E. Schwartz, and R. Ruedy,
839   2008: MATRIX (Multiconfiguration Aerosol TRacker of mIXing state): An aerosol microphysical
840   module for global atmospheric models. Atmos. Chem. Phys., 8, 6603-6035, doi:10.5194/acp-8-6003-
841   2008.
842   Bauer, S. E., K. Tsigaridis, and R. Miller, Significant atmospheric aerosol pollu4on caused by world food
843   cultivation, Geophys. Res. Lett., 43, no. 10, 5394-5400, doi:10.1002/2016GL068354, 2016.
844   Bessagnet, B. and Rouïl, L.: Feedback on and analysis of the PM pollution episode in March 2014,
845   presentation at 19-th EIONET Workshop on Air Quality Assessment and Management Berne,
846   Switzerland, 30 September and 1 October 2014, 2014.
847   Bey, I, D.J. Jacob, R.M. Yantosca, J.A. Logan, B.D. Field, A.M. Fiore, Q. Li, H.Y. Liu, L.J. Mickley, M.G.
848   Schultz, 2001: Global modeling of tropospheric chemistry with assimilated meteorology: Model
849   description and evaluation. J. Geophys. Res., 106, 23073-23078 (2001JD000807.
850   Bellouin, N., Rae, J., Jones, A., Johnson, C., Haywood, J., and Boucher, O.: Aerosol forcing in the Climate
851   Model Intercomparison Project (CMIP5) simulations by HadGEM2-ES and the role of ammonium
852   nitrate, J. Geophys. Res.-Atmos., 116, D20206, doi:10.1029/2011jd016074, 2011.
853   Berntsen, T. K. and Isaksen, I. S. A.: A global three-dimensional chemical transport model for the
854   troposphere.1. Model description and CO and ozone results, J. Geophys. Res.-Atmos., 102(D17), 21
855   239–21 280, 1997.
856   Bian, H., and C. S. Zender (2003), Mineral dust and global tropospheric chemistry: The relative roles of
857   photolysis and heterogeneous uptake. J. Geophys. Res., 108, 4672.
858   Bian, H., Chin, M., Rodriguez, J. M., Yu, H., Penner, J. E., and Strahan, S., 2009: Sensitivity of aerosol
859   optical thickness and aerosol direct radiative effect to relative humidity, Atmos. Chem. Phys., 9, 2375-
860   2386, doi:10.5194/acp-9-2375-2009.
861   Bian, H., Colarco, P. R., Chin, M., Chen, G., Rodriguez, J. M., Liang, Q., Blake, D., Chu, D. A.,
862   da Silva, A., Darmenov, A. S., Diskin, G., Fuelberg, H. E., Huey, G., Kondo, Y., Nielsen, J. E.,
863   Pan, X., and Wisthaler, A.: Source attributions of pollution to the Western Arctic during the NASA
864   ARCTAS field campaign, Atmos. Chem. Phys., 13, 4707-4721, doi:10.5194/acp-13-4707-2013, 2013.
865   Bouwman, A.F., Lee, D.S., Asman, W.A.H., Dentener, F.J., Van Der Hoek, K.W. and J.G.J. Olivier (1997).
866   A Global High-Resolution Emission Inventory for Ammonia, Global Biogeochemical Cycles, 11:4,
867   561-587. http://www.rivm.nl/.
868   Chin, M., P. Ginoux, S. Kinne, B. N. Holben, B. N. Duncan, R. V. Martin, J. A. Logan, A. Higurashi, and
869   T. Nakajima, 2002: Tropospheric aerosol optical thickness from the GOCART model and comparisons
870   with satellite and sun photometer measurements, J. Atmos. Sci. 59, 461-483.

Atmospheric
Chemistry
and Physics
Discussions

871   Cubison, M.J., A.M. Ortega, P.L. Hayes, D.K. Farmer, D.Day, M.J. Lechner, W.H. Brune, E. Apel, G.S.
872   Diskin, J.A. Fisher, H.E. Fuelberg, A. Hecobian, D.J. Knapp, T. Mikoviny, D. Riemer, G.W. Sachse,
873   W. Sessions, R.J. Weber, A.J. Weinheimer, A. Wisthaler, and J.L. Jimenez (2011), Effects of Aging on
874   Organic Aerosol from Open Biomass Burning Smoke in Aircraft & Lab Studies. Atmos. Chem. and
875   Phys. Disc. 11, 12103-12140, doi:10.5194/acpd-11-12103-2011.
876   DeCarlo, P. F., Kimmel, J. R., Trimborn, A., Northway, M. J., Jayne, J. T., Aiken, A. C., Gonin, M.,
877   Fuhrer, K., Horvath, T., Docherty, K. S., Worsnop, D. R., and Jimenez, J. L.: Field-deployable, high-
878   resolution, time-of-flight aerosol mass spectrometer, Anal. Chem., 78(24), 8281–8289, 2006.
879   Dentener, F. J., G. R. Carmichael, Y. Zhang, J. Lelieveld, and P. J. Crutzen, Role of mineral aerosol as a
880   reactive surface in the global troposphere, J. Geophys. Res, 101, 22,869-22889, 1996.
881   Dentener, F., Kinne, S., Bond, T., Boucher, O., Cofala, J., Generoso, S., Ginoux, P., Gong, S., Hoelzemann,
882   J. J., Ito, A., Marelli, L., Penner, J. E., Putaud, J.-P., Textor, C., Schulz, M., van der Werf, G. R., and
883   Wilson, J.: Emissions of primary aerosol and precursor gases in the years 2000 and 1750 prescribed
884   data-sets for AeroCom, Atmos. Chem. Phys., 6, 4321–4344, doi:10.5194/acp-6-4321-2006, 2006.
885   Ensberg, J. J., Craven, J. S., Metcalf, A. R., Allan, J. D., Angevine, W. M., Bahreini, R., Brioude, J., Cai,
886   C., Coe, H., de Gouw, J. A., Ellis, R. A., Flynn, J. H., Haman, C. L., Hayes, P. L., Jimenez, J. L.,
887   Lefer, B. L., Middlebrook, A. M., Murphy, J. G., Neuman, J. A., Nowak, J. B., Roberts, J. M., Stutz, J.,
888   Taylor, J. W., Veres, P. R., Walker, J. M., and Seinfeld, J. H.: Inorganic and black carbon aerosols in
889   the Los Angeles Basin during CalNex, Journal of Geophysical Research-Atmospheres, 118, 1777-
890   1803, 2013.
891   Fairlie, T. D., Jacob, D. J., Dibb, J. E., Alexander, B., Avery, M. A., van Donkelaar, A., and Zhang, L.:
892   Impact of mineral dust onnitrate, sulfate, and ozone in transpacific Asian pollution plumes, Atmos.
893   Chem. Phys., 10, 3999–4012, doi:10.5194/acp-10-3999- 2010, 2010.
894   Feng, Y. and Penner, J. E.: Global modeling of nitrate and ammonium: Interaction of aerosols and
895   tropospheric chemistry, J. Geophys. Res.-Atmos., 112, D01304, doi:10.1029/2005jd006404, 2007.
896   Fenn, M. E., M. A. Poth, D. W. Johnson, Evidence for nitrogen saturation in the San Bernardino Mountains
897   in southern California, Forest Ecology and Management , Volume 82, Issues 1–3, April 1996, Pages
898   211-230.
899   Fitzgerald, J. W. (1975), Approximation formulas for equilibrium size or an aerosol particle as a function
900   of its dry size and composition and ambient relative humidity, J. Appl. Meteorol., 14(6), 1044-1049.
901   Fowler, Z. K., M. B. Adams, W. T. Peterjohn,Will more nitrogen enhance carbon storage in young forest
902   stands in central Appalachia? Forest Ecology and Management, Volume 337, Pages 144–152, 1
903   February 2015.
904   Galloway, J. N., Dentener, F. J., Capone, D. G., Boyer, E. W., Howarth, R. W., Seitzinger, S. P., Asner, G.
905   P., Cleveland, C. C., Green, P. A., Holland, E. A., Karl, D. M., Michaels, A. F., Porter, J. H.,
906   Townsend, A. R. and Vorosmarty, C. J.: Nitrogen cycles: Past, present, and future, Biogeochemistry,
907   70, 153–226, 2004.
908   Ginoux, P., M. Chin, I. Tegen, J. Prospero, B. Holben, O. Dubovik, and S.-J. Lin, 2001: Sources and global
909   distributions of dust aerosols simulated with the GOCART model, J. Geophys. Res., 106, 20,255-
910   20,273.
911   Grieshop, A. P., Robinson, A. L., Duplissy, J., Smith, J. D., Wilson, K. R., Lanz, V. A., Hueglin, C., Sun,
912   Y. L., Tian, J., Laaksonen, A., Raatikainen, T., Rautiainen, J., Vaattovaara, P., Ehn, M., Kulmala, M.,
913   Tomlinson, J. M., Collins, D. R., Cubison, M. J., Dunlea, E. J., Huffman, J. A., Onasch, T. B., Alfarra,
914   M. R., Williams, P. I., Bower, K., Kondo, Y., Schneider, J., Drewnick, F., Borrmann, S., Weimer, 5 S.,
915   Demerjian, K., Salcedo, D., Cottrell, L., Griffin, R., Takami, A., Miyoshi, T., Hatakeyama, S.,
916   Shimono, A., Sun, J. Y., Zhang, Y. M., Dzepina, K., Kimmel, J. R., Sueper, D., Jayne, J. T., Herndon,
917   S. C., Trimborn, A. M., Williams, L. R., Wood, E. C., Middlebrook, A. M., Kolb, C. E., Baltensperger,
918   U., and Worsnop, D. R.: Evolution of organic aerosols in the atmosphere, Science, 326, 1525–1529,
919   2009.
920   Hansell, D.A., Follows, M.J., 2008. Nitrogen in the Atlantic Ocean. In: Mullholland, M., Bronk, D.,
921   Capone, D., Carpenter, E. (Eds.), Nitrogen in the Marine Environment, second ed. Academic Press, pp.
922   597–630.
923   Hauglustaine, D. A., Hourdin, F., Walters, S., Jourdain, L., Filiberti, M.-A., Larmarque, J.-F., and Holland,
924   E. A.: Interactive chemistry in the Laboratoire de Météorologie Dynamique general circulation model:
925   description and background tropospheric chemistry evaluation, J. Geophys. Res., 109, D04314,
926   doi:10.1029/2003JD003957, 2004.

Atmospheric
Chemistry
and Physics
Discussions

Open Access

927   Hauglustaine, D. A., Balkanski, Y., and Schulz, M.: A global model simulation of present and future
928   nitrate aerosols and their direct radiative forcing of climate, Atmos. Chem. Phys., 14, 11031–11063,
929   doi:10.5194/acp-14-11031-2014, 2014.
930   Haywood, J., Bush, M., Abel, S., Claxton, B., Coe, H., Crosier, J., Harrison, M., Macpherson, B., Naylor,
931   M., and Osborne, S.: Prediction of visibility and aerosol within the operational Met Office Unified
932   Model II?: Validation of model performance using observational data, Q. J. Roy. Meteorol. Soc., 134,
933   1817–1832, doi:10.1002/qj.275, 2008.
934   Heald, C. L., Collett Jr., J. L., Lee, T., Benedict, K. B., Schwandner, F. M., Li, Y., Clarisse, L., Hurtmans,
935   D. R., Van Damme, M., Clerbaux, C., Coheur, P.-F., Philip, S., Martin, R. V., and Pye, H. O. T.:
936   Atmospheric ammonia and particulate inorganic nitrogen over the United States, Atmos. Chem. Phys.,
937   12, 10295–10312, doi:10.5194/acp-12-10295-2012, 2012.
938   Hess, M., P. Koepke and I. Schult, Optical properties of aerosols and clouds: The software package OPAC.
939   Bull. Amer. Meteorol. Soc., 79(5): 831-844, 1998.
940   Huffman, J. A., J. T. Jayne, F. Drewnick, A. C. Aiken, T. Onasch, D. R. Worsnop, and J. L. Jimenez,
941   Design, Modeling, Optimization, and Experimental Tests of a Particle Beam Width Probe for the
942   Aerodyne Aerosol Mass Spectrometer, Aerosol Sci Technol. 39, 1143-1163, 2005.
943   Huneeus, N., M. Schulz, Y. Balkanski, J. Griesfeller, S. Kinne, J. Prospero, S. Bauer, O. Boucher, M. Chin,
944   F. Dentener, T. Diehl, R. Easter, D. Fillmore, S. Ghan, P. Ginoux, A. Grini, L. Horowitz, D. Koch,
945   M.C. Krol, W. Landing, X. Liu, N. Mahowald, R.L. Miller, J.-J. Morcrette, G. Myhre, J.E. Penner, J.P.
946   Perlwitz, P. Stier, T. Takemura, and C. Zender, 2011: Global dust model intercomparison in AeroCom
947   phase I. *Atmos. Chem. Phys.*, 11, 7781-7816, doi:10.5194/acp-11-7781-2011.
948   IPCC: (Intergovernmental Panel on Climate Change): The physical science basis. Contribution of working
949   group I to the fifth assessment report of the intergovernmental panel on climate change. T.F. Stocker, D.
950   Qin, G.-K. Plattner, M. Tignor, S.K. Allen, J. Boschung, A. Nauels, Y. Xia, V. Bex, and P.M. Midgley
951   (eds.). Cambridge University Press, Cambridge, United Kingdom and New York, NY, USA, 2013.
952   2013.
953   Jimenez, J. L., Canagaratna, M. R., Donahue, N. M., Prevot, A. S. H., Zhang, Q., Kroll, J. H., DeCarlo, P.
954   F., Allan, J. D., Coe, H., Ng, N. L., Aiken, A. C., Docherty, K. S., Ulbrich, I. M.,
955   Jacob, D. J., Crawford, J. H., Maring, H., Clarke, A. D., Dibb, J. E., Emmons, L. K., Ferrare, R. A.,
956   Hostetler, C. A., Russell, P. B., Singh, H. B., Thompson, A. M., Shaw, G. E., McCauley, E., Pederson,
957   J. R., and Fisher, J. A.: The Arctic Research of the Composition of the Troposphere from Aircraft and
958   Satellites (ARCTAS) mission: design, execution, and first results, Atmos. Chem. Phys., 10, 5191–
959   5212, doi:10.5194/acp-10-5191-2010, 2010.
960   Janssens-Maenhout, G., Crippa, M., Guizzardi, D., Dentener, F., Muntean, M., Pouliot, G., Keating, T.,
961   Zhang, Q., Kurokawa, J., Wankmüller, R., Denier van der Gon, H., Kuenen, J. J. P., Klimont, Z., Frost,
962   G., Darras, S., Koffi, B., and Li, M.: HTAP_v2.2: a mosaic of regional and global emission grid maps
963   for 2008 and 2010 to study hemispheric transport of air pollution, Atmos. Chem. Phys., 15, 11411-
964   11432, doi:10.5194/acp-15-11411-2015, 2015
965   Jöckel, P., Kerkweg, A., Pozzer, A., Sander, R., Tost, H., Riede, H., Baumgaertner, A., Gromov, S., and
966   Kern, B.: Development cycle 2 of the Modular Earth Submodel System (MESSy2), Geosci. Model
967   Dev., 3, 717–752, doi:10.5194/gmd-3-717-2010, 2010.
968   John,W., S. M.Wall, J. L. Ondo, and W. Winklmayr (1989), Acidic-aerosol size distributions during
969   SCAQS (Southern California Air Quality Study), final report, Rep. CA/DOH/AIHL/SP-51, Calif. Air
970   Resour. Board, Sacramento.
971   Kanakidou, M., R.A. Duce, J.M. Prospero, A.R. Baker, C. Benitez-Nelson, F.J. Dentener, K.A. Hunter,
972   P.S. Liss, N. Mahowald, G.S. Okin, M. Sarin, K. Tsigaridis, M. Uematsu, L.M. Zamora, and T. Zhu,
973   2012: Atmospheric fluxes of organic N and P to the global ocean. Glob. Biogeochem. Cycles, 26,
974   GB3026, doi:10.1029/2011GB004277.
975   Kanakidou, M., S. Myriokefalitakis, N. Daskalakis, G. Fanourgakis, A. Nenes, A. Baker, K. Tsigaridis, and
976   N. Mihalopoulos, 2016: Past, present and future atmospheric nitrogen deposition. J. Atmos. Sci., 73,
977   no. 5, 2039-2047, doi:10.1175/JAS-D-15-0278.1.
978   Karydis, V. A., Tsimpidi, A. P., Fountoukis, C., Nenes, A., Zavala, M., Lei, W., Molina, L. T., and Pandis,
979   S. N.: Simulating the fine and coarse inorganic particulate matter concentrations in a polluted
980   megacity, Atmospheric Environment, 44, 608-620, 2010.

Atmospheric
Chemistry
and Physics
Discussions

981 Karydis, V. A., Tsimpidi, A. P., Lei, W., Molina, L. T., and Pandis, S. N.: Formation of semivolatile
982   inorganic aerosols in the Mexico City Metropolitan Area during the MILAGRO campaign,
983   Atmospheric Chemistry and Physics, 11, 13305-13323, 2011.
984 Karydis, V. A., A. P. Tsimpidi, A. Pozzer, M. Astitha, and J. Lelieveld, 2016: Effects of mineral dust on
985   global atmospheric nitrate concentrations. Atmos. Chem. Phys., 16, 1491–1509, doi:10.5194/acp-16-
986   1491-2016.
987 Kim, Y. P., Seinfeld, J. H., and Saxena, P.: Atmospheric gas–aerosol equilibrium I. Thermodynamic model,
988   Aerosol Sci. Technol., 19, 157–181, 1993.
989 Kim, D., M. Chin, H. Yu, T. Diehl, Q. Tan, R.A. Kahn, K. Tsigaridis, S.E. Bauer, T. Takemura, L. Pozzoli,
990   N. Bellouin, M. Schulz, S. Peyridieu, A. Chédin, and B. Koffi, 2014: Sources, sinks, and transatlantic
991   transport of North African dust aerosol: A multi-model analysis and comparison with remote-sensing
992   data. J. Geophys. Res. Atmos., 119, no. 10, 6259-6277, doi:10.1002/2013JD021099.
993 Kinne, S., Schulz, M., Textor, C., Guibert, S., Balkanski, Y., Bauer, S. E., Berntsen, T., Berglen, T. F.,
994   Boucher, O., Chin, M., Collins, W., Dentener, F., Diehl, T., Easter, R., Feichter, J., Fillmore, D., Ghan,
995   S., Ginoux, P., Gong, S., Grini, A., Hendricks, J., Herzog, M., Horowitz, L., Isaksen, I., Iversen, T.,
996   Kirkevåg, A., Kloster, S., Koch, D., Kristjansson, J. E., Krol, M., Lauer, A., Lamarque, J. F., Lesins,
997   G., Liu, X., Lohmann, U., Montanaro, V., Myhre, G., Penner, J., Pitari, G., Reddy, S., Seland, O.,
998   Stier, P., Takemura, T., and Tie, X.: An AeroCom initial assessment – optical properties in aerosol
999   component modules of global models, Atmos. Chem. Phys., 6, 1815–1834, doi:10.5194/acp-6-1815-
1000   2006, 2006.
1001 Koch, D., M. Schulz, S. Kinne, C. McNaughton, J.R. Spackman, T.C. Bond, Y. Balkanski, S. Bauer, T.
1002   Berntsen, O. Boucher, M. Chin, A. Clarke, N. De Luca, F. Dentener, T. Diehl, O. Dubovik, R. Easter,
1003   D.W. Fahey, J. Feichter, D. Fillmore, S. Freitag, S. Ghan, P. Ginoux, S. Gong, L. Horowitz, T. Iversen,
1004   A. Kirkevåg, Z. Klimont, Y. Kondo, M. Krol, X. Liu, R.L. Miller, V. Montanaro, N. Moteki, G.
1005   Myhre, J.E. Penner, J.P. Perlwitz, G. Pitari, S. Reddy, L. Sahu, H. Sakamoto, G. Schuster, J.P.
1006   Schwarz, Ø. Seland, P. Stier, N. Takegawa, T. Takemura, C. Textor, J.A. van Aardenne, and Y. Zhao,
1007   2009: Evaluation of black carbon estimations in global aerosol models. Atmos. Chem. Phys., 9, 9001-
1008   9026, doi:10.5194/acp-9-9001-2009.
1009 Kinnison, D. E., P. S. Connell, J. Rodriguez, D. B. Considine, D. A. Rotman, J. Tannahill, R. Ramaroson,
1010   A. Douglass, S. Baughcum, L. Coy, P. Rasch, D. Waugh, 2001: The Global Modeling Initiative
1011   assessment model: Application to high-speed civil transport perturbation, J. Geophys. Res., 106, 1693-
1012   1712.
1013 Lacis, A. A., Refractive Indices of Three Hygroscopic Aerosols and their Dependence on Relative
1014   Humidity, http://gacp.giss.nasa.gov/data_sets/lacis/introduction.pdf.
1015 Lamarque, J.-F., J. T. Kiehl, G. P. Brasseur, T. Butler, P. Cameron-Smith, et al. (2005), Assessing future
1016   nitrogen deposition and carbon cycle feedback using a multimodel approach : Analysis of nitrogen
1017   deposition, J. of Geophys. Res., Vol. 110, D19303, doi: 10.1029/2005JD005825.
1018 Lee, T., X.-Y. Yu, B. Ayres, S. M. Kreidenweis, W. C. Malm, J. L. Collett Jr., Observations of fine and
1019   coarse particle nitrate at several rural locations in the United States, Atmospheric Environment 42,
1020   2720–2732, 2008.
1021 Li, J., W.-C. Wang, H. Liao, and W. Chang. 2014. Past and future direct radiative forcing of nitrate aerosol
1022   in East Asia. Theor. Appl. Climatol. 1–14. doi:10.1007/s00704-014-1249-1.
1023 Liao, H., P. J. Adams, S. H. Chung, J. H. Seinfeld, L. J. Mickley, and D. J. Jacob (2003), Interactions
1024   between tropospheric chemistry and aerosols in a unified general circulation model, J. Geophys. Res.,
1025   108(D1), 4001, doi:10.1029/2001JD001260.
1026 Liu, X., J. E. Penner, S. J. Ghan, and M. Wang, 2007: Inclusion of Ice Microphysics in the NCAR
1027   Community Atmospheric Model Version 3 (CAM3). J. Climate, 20, 4526-4547.
1028 Liu, Y., G. Gibson, C. Cain, H. Wang, G. Grassian, and A. Laskin (2008) Kinetics of Heterogeneous
1029   Reaction of CaCO3Particles with Gaseous HNO3 over a Wide Range of Humidity, J. Physical
1030   Chemistry A, doi:10.1021/jp076169h
1031 Malm, W. C., Schichtel, B. A., Pitchford, M. L., Ashbaugh, L. L., and Eldred, R. A.: Spatial and monthly
1032   trends in speciated fine particle concentration in the United States, J. Geophys. Res. Atmos., 109(D3),
1033   D03306, doi:10.1029/2003/JD003739, 2004.
1034 Metzger, S., F. Dentener, S. Pandis, and J. Lelieveld (2002), Gas/aerosol partitioning: 1. A computationally
1035   efficient model, J. of Geophys. Res. Vol. 107, No. D16, 4312, 10.1029/2001JD001102.

Atmospheric
Chemistry
and Physics
Discussions

Open Access

EGU

1036 Mezuman, K., S.E. Bauer, and K. Tsigaridis, 2016: Evaluating secondary inorganic aerosols in three
1037   dimensions. Atmos. Chem. Phys., 16, 10651-10669, doi:10.5194/acp-16-10651-2016.
1038 Milegroet, H. Van and D. W. Cole, The Impact of Nitrification on Soil Acidification and Cation Leaching
1039   in a Red Alder Ecosystem, ACSESS, Alliance of Crop, Soil, and Environmental Science Societies,
1040   doi:10.2134/jeq1984.00472425001300040015x ,1984
1041 Myhre, G., A. Grini, and S. Metzger (2006), Modeling of nitrate and ammonium-containing aerosols
1042   inpresence of sea salt, Atmos. Chem. Phys., 6, 4809-4821, www.atmos-chem-phys.net/6/4809/2006/.
1043 Myhre, G., B. H., Samset, M. Schulz, Y. Balkanski, S. Bauer, T. K. Berntsen, H. Bian, N. Bellouin, M.
1044   Chin, T. Diehl, R. C. Easter, J. Feichter, S. J. Ghan, D. Hauglustaine, T. Iversen, S. Kinne, A.
1045   Kirkevåg, J.-F. Lamarque, G. Lin, X. Liu, G. Luo, X. Ma, J. E. Penner, P. J. Rasch, Ø. Seland, R. B.
1046   Skeie, P. Stier, T. Takemura, K. Tsigaridis, Z. Wang, L. Xu, H. Yu, F. Yu, J.-H. Yoon, K. Zhang, H.
1047   Zhang, and C. Zhou, Radiative forcing of the direct aerosol effect from AeroCom Phase II simulations,
1048   Atmos. Chem. Phys., 13, 1853-1877, doi:10.5194/acp-13-1853-2013, 2013.
1049 Nowak, J., J. B., Weinheimer, A. J., Hoff, R. M., Berkoff, T. A., Beyersdorf, A. J., Olson, J., Crawford, J.
1050   H., and Cohen, R. C.: On the effectiveness of nitrogen oxide reductions as a control over ammonium
1051   nitrate aerosol, Atmos. Chem. Phys., 16, 2575–2596, doi:10.5194/acp-16-2575-2016, 2016
1052 Paulot, F., Ginoux, P., Cooke, W. F., Donner, L. J., Fan, S., Lin, M.-Y., Mao, J., Naik, V., and Horowitz, L.
1053   W.: Sensitivity of nitrate aerosols to ammonia emissions and to nitrate chemistry: implications for
1054   present and future nitrate optical depth, Atmos. Chem. Phys., 16, 1459–1477, doi:10.5194/acp-16-
1055   1459-2016, http://www.atmos-chem-phys.net/16/1459/2016/, 2016.
1056 Phoenix, G., W. K. Hicks, S. Cinderby, J. C. I. Kuylenstierna, W. D. Stock, et al. (2006), Atmospheric
1057   nitrogen deposition in world biodiversity hotspots: the need for a greater global perspective in
1058   assessing N deposition impacts, Global Change Biology, 12, 470-476, doi: 10.1111/j.1365-
1059   2486.2006.01104.x.
1060 Prentice, M. J., et al. (2001), The carbon cycle and atmospheric carbon dioxide, in Climate Change 2001,
1061   pp. 184-237, Cambridge Univ. Press, New York.
1062 Pringle, K. J., Tost, H., Message, S., Steil, B., Giannadaki, D., Nenes, A., Fountoukis, C., Stier, P., Vignati,
1063   E., and Leieved, J.: Description and evaluation of GMXe: a new aerosol submodel for global
1064   simulations (v1), Geoscientific Model Development, 3, 391-412, 2010.
1065 Pusede, S. E., Duffey, K. C., Shusterman, A. A., Saleh, A., Laughner, J. L., Wooldridge, P. J., Zhang, Q.,
1066   Parworth, C. L., Kim, H., Capps, S. L., Valin, L. C., Cappa, C. D., Fried, A., Walega, Riemer, N., H.
1067   Vogel, B. Vogel, B. Schell, I. Ackermann, C. Kessler, and H. Hass (2003), Impact of the
1068   heterogeneous hydrolysis of N2O5 on chemistry and nitrate aerosol formation in the lower troposphere
1069   under photosmog conditions, J. Geophys. Res., 108(D4), 4144, doi:10.1029/2002JD002436.
1070 Sander, S. P., J. Abbatt, J. R. Barker, J. B. Burkholder, R. R. Friedl, D. M. Golden, R. E. Huie, C. E. Kolb,
1071   M. J. Kurylo, G. K. Moortgat, V. L. Orkin and P. H. Wine "Chemical Kinetics and Photochemical
1072   Data for Use in Atmospheric Studies, Evaluation No. 17," JPL Publication 10-6, Jet Propulsion
1073   Laboratory, Pasadena, 2011 http://jpldataeval.jpl.nasa.gov.
1074 Saxena, P., Hudischeyskyj, A. B., Seigneur, C., and Seinfeld, J. H., A comparative study of
1075   equilibrium approaches to the chemical characterization of secondary aerosols, Atmos. Enuiron.
1076   20:1471- 1483, 1986.
1077 Schaap, M., Müller, K., & Ten Brink, H. M. (2002). Constructing the European aerosol nitrate
1078   concentration field from quality analysed data. Atmospheric Environment, 36(8), 1323-1335.
1079 Schaap, M., van Loon, M., ten Brink, H. M., Dentener, F. J., and Builtjes, P. J. H.: Secondary
1080   inorganic aerosol simulations for Europe with special attention to nitrate, Atmos. Chem. Phys., 4,
1081   857-874, doi:10.5194/acp-4-857-2004, 2004.
1082 Schmidt, G.A., M. Kelley, L. Nazarenko, R. Ruedy, G.L. Russell, I. Aleinov, M. Bauer, S.E. Bauer,
1083   M.K. Bhat, R. Bleck, V. Canuto, Y.-H. Chen, Y. Cheng, T.L. Clune, A. Del Genio, R. de
1084   Fainchtein, G. Faluvegi, J.E. Hansen, R.J. Healy, N.Y. Kiang, D. Koch, A.A. Lacis, A.N.
1085   LeGrande, J. Lerner, K.K. Lo, E.E. Matthews, S. Menon, R.L. Miller, V. Oinas, A.O. Oloso, J.P.
1086   Perlwitz, M.J. Puma, W.M. Putman, D. Rind, A. Romanou, M. Sato, D.T. Shindell, S. Sun, R.A.
1087   Syed, N. Tausnev, K. Tsigaridis, N. Unger, A. Voulgarakis, M.-S. Yao, and J. Zhang, 2014:
1088   Configuration and assessment of the GISS ModelE2 contributions to the CMIP5 archive. J. Adv.
1089   Model. Earth Syst., 6, no. 1, 141-184, doi:10.1002/2013MS000265.

Atmospheric
Chemistry
and Physics
Discussions

1090 Schulz, M., Textor, C., Kinne, S., Balkanski, Y., Bauer, S., Berntsen, T., Berglen, T., Boucher, O.,
1091   Dentener, F., Guibert, S., Isaksen, I. S. A., Iversen, T., Koch, D., Kirkevåg, A., Liu, X.,
1092   Montanaro, V., Myhre, G., Penner, J. E., Pitari, G., Reddy, S., Seland, Ø., Stier, P., and
1093   Takemura, T.: Radiative forcing by aerosols as derived from the AeroCom present-day and pre-
1094   industrial simulations,Atmos. Chem. Phys., 6, 5225–5246, doi:10.5194/acp-6-5225-2006, 2006.
1095 Schutgens, N. A. J., Gryspeerdt, E., Weigum, N., Tsyro, S., Goto, D., Schulz, M. and Stier, P.: Will a
1096   perfect model agree with perfect observations? The impact of spatial sampling, Atmos. Chem.
1097   Phys., 16(10), 6335-6353, 2016.
1098 Shindell, D. T., Faluvegi, G., and Bell, N.: Preindustrial-to-present-day radiative forcing by
1099   tropospheric ozone from improved simulations with the GISS chemistry-climate GCM, Atmos.
1100   Chem. Phys., 3, 1675–1702, 2003.
1101 Simpson, D., Benedictow, A., Berge, H., Bergström, R., Emberson, L. D., Fagerli, H., Flechard, C. R.,
1102   Hayman, G. D., Gauss, M., Jonson, J. E., Jenkin, M. E., Nyíri, A., Richter, C., Semeena, V. S., Tsyro,
1103   S., Tuovinen, J. P., Valdebenito, Á., and Wind, P.: The EMEP MSC-W chemical transport model -
1104   technical description, Atmos. Chem. Phys., 12, 7825-7865, 10.5194/acp-12-7825-2012, 2012.
1105 Song, C. H., and G. R. Carmichael, Gas-particle partitioning of nitric acid modulated by alkaline aerosol, J.
1106   Atmos. Chem., 40, 1–22, 2001.
1107 Strahan, S. E., Duncan, B. N., and Hoor, P.: Observationally derived transport diagnostics for the
1108   lowermost stratosphere and their application to the GMI chemistry and transport model, Atmos. Chem.
1109   Phys., 7, 2435-2445, doi:10.5194/acp-7-2435-2007, 2007.
1110 Sudo, K., M. Takahashi, J. Kurokawa, and H. Akimoto, CHASER: A global chemical model of the
1111   troposphere, 1. Model description, J. Geophys. Res., 107(D17), 4339, doi:10.1029/2001JD001113,
1112   2002.
1113 Takiguchi, Y., A. Takami, Y. Sadanaga, X. Lun, A. Shimizu, I. Matsui, N. Sugimoto, W. Wang, H.
1114   Bandow, and S. Hatakeyama (2008), Transport and transformation of total reactive nitrogen over the
1115   East China Sea, J. Geophys. Res., 113, D10306, doi:10.1029/2007JD009462.
1116 Textor, C., Schulz, M., Guibert, S., Kinne, S., Balkanski, Y., Bauer, S., Berntsen, T., Berglen, T., Boucher,
1117   O., Chin, M., Dentener, F., Diehl, T., Easter, R., Feichter, H., Fillmore, D., Ghan, S., Ginoux, P.,
1118   Gong, S., Grini, A., Hendricks, J., Horowitz, L., Huang, P., Isaksen, I., Iversen, I., Kloster, S., Koch,
1119   D., Kirkevåg, A., Kristjansson, J. E., Krol, M., Lauer, A., Lamarque, J. F., Liu, X., Montanaro, V.,
1120   Myhre, G., Penner, J., Pitari, G., Reddy, S., Seland, Ø., Stier, P., Takemura, T., and Tie, X.: Analysis
1121   and quantification of the diversities of aerosol life cycles within AeroCom, Atmos. Chem. Phys., 6,
1122   1777–1813, doi:10.5194/acp-6-1777-2006, 2006.
1123 Tost, H., Jöckel, P., Kerkweg, A., Sander, R., and Lelieveld, J.: Technical note: A new comprehensive
1124   SCAVenging submodel for global atmospheric chemistry modelling, Atmos. Chem. Phys., 6, 565-574,
1125   doi:10.5194/acp-6-565-2006, 2006.
1126 Trail, M., Tsimpidi, A. P., Liu, P., Tsigaridis, K., Rudokas, J., Miller, P., Nenes, A., Hu, Y., and Russell, A.
1127   G.: Sensitivity of air quality to potential future climate change and emissions in the United States and
1128   major cities, Atmospheric Environment, 94, 552-563, 2014.
1129 Trump, E. R., Fountoukis, C., Donahue, N. M., and Pandis, S. N.: Improvement of simulation of fine
1130   inorganic PM levels through better descriptions of coarse particle chemistry, Atmospheric
1131   Environment, 102, 274-281, 2015.
1132 Tsigaridis, K., Daskalakis, N., Kanakidou, M., Adams, P. J., Artaxo, P., Bahadur, R., Balkanski, Y.,
1133   Bauer, S. E., Bellouin, N., Benedetti, A., Bergman, T., Berntsen, T. K., Beukes, J. P., Bian, H.,
1134   Carslaw, K. S., Chin, M., Curci, G., Diehl, T., Easter, R. C., Ghan, S. J., Gong, S. L., Hodzic, A.,
1135   Hoyle, C. R., Iversen, T., Jathar, S., Jimenez, J. L., Kaiser, J. W., Kirkevåg, A., Koch, D., Kokkola, H.,
1136   Lee, Y. H, Lin, G., Liu, X., Luo, G., Ma, X., Mann, G. W., Mihalopoulos, N., Morcrette, J.-J.,
1137   Müller, J.-F., Myhre, G., Myriokefalitakis, S., Ng, N. L., O'Donnell, D., Penner, J. E., Pozzoli, L.,
1138   Pringle, K. J., Russell, L. M., Schulz, M., Sciare, J., Seland, Ø., Shindell, D. T., Sillman, S.,
1139   Skeie, R. B., Spracklen, D., Stavrakou, T., Steenrod, S. D., Takemura, T., Tiitta, P., Tilmes, S.,
1140   Tost, H., van Noije, T., van Zyl, P. G., von Salzen, K., Yu, F., Wang, Z., Wang, Z., Zaveri, R. A.,
1141   Zhang, H., Zhang, K., Zhang, Q., and Zhang, X.: The AeroCom evaluation and intercomparison of
1142   organic aerosol in global models, Atmos. Chem. Phys., 14, 10845-10895, doi:10.5194/acp-14-10845-
1143   2014, 2014.

Atmospheric
Chemistry
and Physics
Discussions

1144   Tsimpidi, A. P., Karydis, V. A., and Pandis, S. N.: Response of inorganic fine particulate matter to
1145   emission changes of sulfur dioxide and ammonia: The eastern United States as a case study, Journal of
1146   the Air & Waste Management Association, 57, 1489-1498, 2007.
1147   Tsimpidi, A. P., Karydis, V. A., and Pandis, S. N.: Response of Fine Particulate Matter to Emission
1148   Changes of Oxides of Nitrogen and-Anthropogenic Volatile Organic Compounds in the Eastern United
1149   States, Journal of the Air & Waste Management Association, 58, 1463-1473, 2008.
1150   Vieno, M., Heal, M. R., Twigg, M. M., MacKenzie, I. A., Braban, C. F., Lingard, J. J. N. Ritchie, S., Beck,
1151   R. C., A., M., Ots, R., DiMarco, C. F., Nemitz, E., Sutton, M. A., and Reis, S.: The UK particulate
1152   matter air pollution episode of March-April 2014: more than Saharan dust., Environ. Res. Lett.,
1153   doi:10.1088/1748-9326/11/4/044004, 2016.
1154   Walker, J. M., Philip, S., Martin, R. V., and Seinfeld, J. H.: Simulation of nitrate, sulfate, and ammonium
1155   aerosols over the United States, Atmos. Chem. Phys., 12, 11213–11227, doi:10.5194/acp-12-11213-
1156   2012, 2012.
1157   Watanabe, S., T. Hajima, K. Sudo, T. Nagashima, T. Takemura, H. Okajima, *et al*. MIROC-ESM 2010:
1158   model description and basic results of CMIP5-20c3m experiments, Geosci. Model Dev., 4 (2011), pp.
1159   845–872.
1160   Williams, E. J., S. T. Sandholm, J. D. Bradshaw, J. S. Schendel, A. O. Langford, P. K. Quinn, P. J. LeBel,
1161   S. A. Vay, P. D. Roberts, R. B. Norton, B. A. Watkins, M. P. Buhr, D. D. Parrish, J. G. Calvert, and F.
1162   C. Fehsenfeld, An intercomparison of five ammonia measurement techniques, J. Geophys. Res., Vol.,
1163   97, No. D11, Pages 11591-11611, July 20, 1992.
1164   van der Werf, G. R., Randerson, J. T., Giglio, L., Collatz, G. J., Mu, M., Kasibhatla, P. S., Morton, D. C.,
1165   DeFries, R. S., Jin, Y., and van Leeuwen, T. T.: Global fire emissions and the contribution of
1166   deforestation, savanna, forest, agricultural, and peat fires (1997–2009), Atmos. Chem. Phys., 10,
1167   11707-11735, doi:10.5194/acp-10-11707-2010, 2010.
1168   Zender, C. S., Bian, H. S., and Newman, D.: Mineral Dust Entrainment and Deposition (DEAD) model:
1169   Description and 1990s dust climatology, J. Geophys. Res.-Atmos., 108, 4416,
1170   doi:10.1029/2002jd002775, 2003.
1171   Zhou, J., B. Gu, W. H. Schlesinger, X. Ju, Significant accumulation of nitrate in Chinese semi-humid
1172   croplands, Scientific Reports 6, Article number: 25088, doi:10.1038/srep25088, 2016.
1173
1174
1175
1176
1177
1178
1179
1180
1181
1182
1183
1184
1185
1186
1187
1188
1189
1190
1191
1192
1193

1194 **Table 1. Nitrate chemical mechanism and physical properties of AeroCom**
1195 **models**

Model	CHEM-EQM	HNO3 chem mechanism	CHEM DUST	CHEM SEASALT	How do CHEMDUSS	Bins for nitrate	Model Name & resolution	References
CHASER	ISORROPIA-I	CHASER (Sudo et al., 2002)	No	No	---	Fine mode	MIROC, GCM, 2.8°x2.8°x64	Watanabe et al., 2011
EMAC	ISORROPIA-II (Stable state[a])	MESSy2 (Jöckel et al., 2010)	Yes	Yes	ISORROPIA-II	4 bins: Nucleation, Aitken, Accumulation, Coarse	ECHAM5, GCM, 2.8°x2.8°x31	Karydis et al., 2016
EMEP	MARS	EMEP EmChem09 (Simpson et al., 2012)	Yes	Yes	First order loss	Fine and coarse	ECMWF-IFS, CTM, 0.5x0.5°x20	Simpson et al., 2012
GMI	RPMARES (Stable state)	GMI (Straham et al., 2007)	Yes	Yes	first order loss	3 bins: (D<0.1, 0.1 – 2.5, > 2.5 um)	MERRA2, CTM, 2.5°x2°x72	Bian et al., 2009
INCA	INCA (Stable state)	INCA tropospheric chemistry (Hauglustaine et al., 2004)	Yes	Yes	first order loss	2 bins : (D< 1µm and 1 - 10µm)	LMD-v4, GCM, 1.9°x3.75°x39	Hauglustaine et al., 2014
GISS MATRIX	ISORROPIA-II (Stable state)	MATRIX Bauer (2008) and tropospheric chemistry (Shindell et al., 2003)	No	No	NO	Distributed over all mixing states e.g. size distributions.	NASA GISS-E2, GCM, 2°x2.5°x40	Schmidt et al 2014
GISS OMA	EQSAM_v03d (Metastable[b])	OMA (Bauer 2007) and tropospheric chemistry (Shindell et al., 2003)	Yes	No	Bauer and Koch, 2005	Fine mode	NASA GISS-E2, GCM, 2°x2.5°x40	Schmidt et al 2014
Oslo CTM2	EQSAM_v03d (Metastable)	Oslo CTM2 (Berntsen and Isaksen, 1997)	No	Yes	EQSAM_v03d	2 bins: fine and coarse mode	ECMWF, CTM, 2.8°x2.8°x60	Myhre et al., 2006
Oslo CTM3	EQSAM_v03d (Metastable)	Oslo CTM2 (Berntsen and Isaksen, 1997)	No	Yes	EQSAM_v03d	2 bins: fine and coarse mode	ECMWF, CTM, 2.25°x2.25°x60	Myhre et al., 2006

1196 [a]Stable state: where salts precipitate once the aqueous phase becomes saturated
1197 [b]Metastable: where the aerosol is composed only of a supersaturated aqueous phase
1198
1199 **Table 2. Characteristics of thermodynamic equilibrium models**

	ISORROPIA-I	ISORROPIA-II	MARS	RPMARES	INCA	EQSAM_v03d
Species	Sulfate, nitrate, ammonium, sodium, chloride	Sulfate, nitrate, ammonium, sodium, chloride, crustal species	Sulfate, nitrate, ammonium	Sulfate, nitrate, ammonium	Sulfate, nitrate, ammonium	Sulfate, nitrate, ammonium, sodium, chloride
# of components	23	34	16	11	9	18
# of reactions	15	27	7	6	4	25
Multicomponent activity coefficient	Bromley	Bromley	Bromley	Bromley	Seinfeld and Pandis	Metzger
Binary activity coefficient	Kusik and Meissner	Kusik and Meissner	Pitzer	Pitzer	Seinfeld and Pandis	Metzger
Water activity	ZSR[a]	ZSR	ZSR	ZSR		ZSR
Kelvin effect	No	No	No	No	No	No
Quantities that determine subdomains	$[Na^+]$, $[NH_4^+]$, $[SO_4^{2-}]$	$[Ca^{2+}]$, $[K^+]$, $[Mg^{2+}]$, $[Na^+]$, $[NH_4^+]$, $[SO_4^{2-}]$	RH, $[NH_4^+]$, $[SO_4^{2-}]$	$[NH_4^+]$, $[SO_4^{2-}]$	$[NH_4^+]$, $[SO_4^{2-}]$	$[NH_4^+]$, $[SO_4^{2-}]$
# of subdomains	4	5	4	2	3	3

Atmospheric
Chemistry
and Physics
Discussions

1200   [a]ZSR: *Zdanovskii-Stokes-Robinson*

1201

1202   **Table3. Summary of the observational data used in this study**

SURFACE NETWORK	QUANTITY	COVER AREA	# of sites in 2008	SAMPLE FREQUENCE	SOURCE
CASTNET	Concentration of HNO_3, NO_3^-, NH_4^+, SO_4^{2-} Dry deposition of them	North America	83	weekly	www.epa.gov/castnet/ clearsession.do
AMoN	Concentration of NH_3	U.S.	19	2-weekly	http://nadp.isws.illinois.edu/
NADP/NTN	Wet deposition of $HNO_3+NO_3^-$, NH_4^+, SO_4^{2-}	U.S.	253	weekly	nadp.isws.illinois.edu
EMEP	Concentration of HNO_3, NH_3, NO_3^-, NH_4^+, SO_4^{2-}	Europe	35	daily	http://www.nilu.no/projects/ccc/index.html
EANET	Concentration of HNO_3, NH_3, NO_3^-, NH_4^+, SO_4^{2-}	East Asia	56	Daily to 2-weekly	http://www.eanet.asia/eanet/brief.html
	Wet deposition of $HNO_3+NO_3^-$, NH_4^+, SO_4^{2-}			24 hours or precipitation event	
AIRCRAFT CAMPAIGNS	QUANTITY	COVER AREA	# of Flights	CAMPAIGN PERIOD	SOURCE
ARCTAS-A	Concentration of NO_3^-, NH_4^+, SO_4^{2-}	Alaska, U.S.	11	March-April	http://www-air.larc.nasa.gov/cgi-bin/arcstat-c
ARCTAS-CARB		California Bay area U.S.	6	June	
ARCTAS-B		Central Canada	7	July	

1203

1204

1205   **Table 4a. NO_3^- global budget for each model**

Tracer	Model	Burden (Tg)	SConc (µg kg⁻¹)	DDep (Tg a⁻¹)	WDep (Tg a⁻¹)	ChemDUSS[a] (Tg a⁻¹)	ChemP[a] (Tg a⁻¹)	Lifetime (days)	AOD[b]
NO_3^-	CHASER	0.16	0.18	-	-	-	-	-	0.0076
	EMAC	0.67	0.47	46.3	-		-	-	-
	EMEP	0.96	0.30	15.0	62.7	(71.7)[c]	4.5	4.5	0.0073
	GISS-MATRIX	0.22	0.06	1.3	9.6	(10.9)		7.4	-
	GISS-OMA	0.14	0.05	1.1	5.5	(6.6)		7.8	0.0153
	GMI	0.26	0.22	14.9	31.5	41.9	4.8	2.1	0.0047
	INCA	0.79	0.17	4.5	44.6	44.1	9.8	5.9	0.0064
	Oslo-CTM2	0.60	0.25	47.8	61.5	(109.3)		2.0	0.0018
	Oslo-CTM3	1.88	0.36	34.6	90.6	(125.2)		5.5	-
	Avg	0.63	0.23	20.7	45.9	60.6		5.0	0.0072
	Med	0.60	0.22	15.0	44.6	46.7		5.5	0.0064
	Ratio[d]	13.4	9.4	43.5	16.5	19.0		3.9	8.5

1206   [a]: ChemDUSS and ChemP refer to NO_3^- chemical production associated with dust/sea
1207   salt and NH_3/NH_4^+, respectively

1208   [b]: AOD here includes NH_4^+ that is associated to NO_3^- for all models expect EMEP

1209   [c]: value inside parenthesis is estimated total NO_3^- chemical production based on its
1210   total loss, while budget without parenthesis is reported directly by model.

1211   [d]: a ratio between maximum to minimum model simulations

1212

1213

Atmospheric
Chemistry
and Physics
Discussions

1214   **Table 4b NH$_3$ and NH$_4^+$ global budget for each model**

Tracer	Model	Emi (Tg a^{-1})	Burden (Tg)	SConc (µg kg^{-1})	DDep (Tg a^{-1})	WDep (Tg a^{-1})	ChemP/L (Tg a^{-1})	Lifetime (days)	AOD
NH$_4^+$	CHASER		0.75	0.44	20.9	7.2	(28.1)[a]	9.8	-
	EMAC		0.19	0.12	3.6	44.5[b]	-	-	-
	EMEP		0.20	0.15	4.0	26.4	(30.4)	2.4	0.0059
	GISS-MATRIX		0.31	0.18	4.1	27.9	(32.0)	3.5	-
	GISS-OMA		0.31	0.19	4.2	24.0	(28.2)	4.0	-
	GMI		0.17	0.14	1.7	30.6	32.2	1.9	-
	INCA		0.39	0.08	2.4	20.4	22.9	6.3	-
	Oslo-CTM2		0.29	0.14	5.3	32.6	(37.9)	2.8	-
	Oslo-CTM3		0.30	0.16	5.6	26.1	(31.7)	3.5	-
	Avg		0.32	0.18	5.8	24.4[c]	30.4	4.3	
	Med		0.30	0.15	4.1	26.3[c]	31.1	3.5	
	Ratio		4.4	5.5	12.3	4.5[c]	1.7	5.2	
NH$_3$	CHASER	62.8	0.13	0.46	19.8	6.8	(36.2)[a]	0.76	
	EMAC	59.3	0.85	1.39	15.5	-	-	-	
	EMEP	56.9	0.09	0.46	15.4	18.2	(33.6)	0.98	
	GISS-MATRIX	63.4[d]	0.17	0.26	18.1	13.4	(31.9)	0.98	
	GISS-OMA	63.4[d]	0.17	0.25	18.4	16.7	(28.3)	0.98	
	GMI	60.4	0.11	0.40	12.6	17.5	30.4	0.67	
	INCA	70.5[d]	0.12	0.39	29.3	18.6	22.4	0.62	
	Oslo-CTM2	65.9	0.08	0.27	15.8	8.1	(42.0)	0.44	
	Oslo-CTM3	63.3	0.05	0.51	23.7	7.7	(31.9)	0.29	
	Avg	62.9	0.20	0.49	18.7	13.4	32.1	0.72	
	Med	63.3	0.12	0.40	18.1	15.1	31.9	0.72	
	Ratio	1.2	17.0	5.6	2.3	2.7	1.9	3.4	

1215   [a] chemical budgets inside parenthesis are inferred based on the reported emission
1216   and total deposition
1217   [b] EMAC gives total wet deposition of NH$_4^+$ and NH$_3$
1218   [c] Statistic values of NH$_4^+$ wet deposition do not include EMAC
1219   [d] INCA uses ECLIPSE anthropogenic emissions, two GISS models use CMIP5
1220   anthropogenic emission, and all other models use HTAPv2 anthropogenic emissions
1221

1222   **Table 4c. HNO$_3$ global budget for each model**

Tracer	Model	Burden[a] (Tg)	SConc (µg kg^{-1})	DDep (Tg a^{-1})	WDep (Tg a^{-1})	CheAP (Tg a^{-1})	CheGP (Tg a^{-1})	CheAL (Tg a^{-1})	CheGL (Tg a^{-1})	Lifetime (days)
HNO$_3$	CHASER	1.1	0.29	74.0[a]	120.9[b]	-	-	-	-	-
	EMAC	3.1	0.32	56.1	136.0[b]	-	-	-	-	-
	EMEP	0.66	0.04	39.2	123.9	-	-	-	-	-
	GISS-MATRIX	5.7	0.12	61.7	167.5	-	-	-	-	-
	GISS-OMA	5.3	0.10	49.8	148.2	-	-	-	-	-
	GMI	1.8	0.18	39.7	128.1	128.1	413	42.6	299	3.5
	INCA	1.5	0.09	47.7	77.5	21	369	10.0	210	5.7
	Oslo-CTM2	1.3	0.05	36.1	66.0					
	Oslo-CTM3	2.3	0.04	36.0	49.3	-	-	-	-	-
	Avg	2.5	0.14	45.8[b]	108.7[c]					
	Med	1.8	0.10	43.7[b]	123.9[c]					

Atmospheric
Chemistry
and Physics
Discussions
Open Access
EGU

	Ratio	8.6	8.0	1.6[b]	3.4[b]

1223 [a]HNO3 burden for the atmosphere up to 100 hPa
1224 [b]for both HNO_3 and NO_3^-
1225 [c]statistical values do not include CHASER and EMAC that report total dry or wet
1226 deposition of HNO_3 and NO_3^-
1227
1228 **Table 4d. SO_4^{2-} global budget for each model**

Tracer	Model	Emi SO2 (Tg a⁻¹)	Emi SO4 (Tg a⁻¹)	Burden (Tg)	SConc (µg kg⁻¹)	DDep (Tg a⁻¹)	WDep (Tg a⁻¹)	Chem GP (Tg a⁻¹)	Chem AqP (Tg a⁻¹)	Lifetime (days)	AOD
SO_4^{2-}	CHASER	111	0	3.3	1.44	22.1	137	(159)		7.6	0.0826
	EMAC	138	619[a]	1.9	1.72	504[b]	302	(187)		0.86	-
	EMEP	109	0	0.83	0.45	10.2	109	(119)		2.5	0.0232
	GISS-MATRIX	133	5.1	1.3	0.63	16.6	97	(109)		4.2	-
	GISS-OMA	133	5.1	1.1	0.53	11.8	112	52.7	66.2	3.3	0.0714
	GMI	111	0	1.1	0.58	7.5	205	126.5	86.1	3.6	0.0257
	INCA	116.	8.0	1.8	0.34	8.4	116	42.2	75.1	5.3	0.0417
	Oslo-CTM2	133	4.1	2.0	0.49	17.6	184	(198)		3.6	0.0366
	Oslo-CTM3	133	4.1	2.7	0.55	20.2	160	(176)		5.5	
	Avg[c]	122		1.8	0.63	14.3	140	151		4.5	0.0469
	Med[c]	133		1.6	0.54	14.2	127	139		3.9	0.0392
	Ratio[c]	1.2		4.0	4.2	2.9	2.1	2.0		3.0	3.6

1229 [a] EMAC emission also includes sea spray SO_4^{2-}
1230 [b] EMAC dry deposition includes sedimentation and SO_4^{2-} sedimentation is very high
1231 since it has assumed that 7.7% of sea salt is SO_4^{2-}
1232 [c] Statistical values do not include EMAC
1233
1234 **Table 5: Effective Henry Law constant used in the models**

Aerocom Model	$H^{\ominus *}$ (M/atm)	$-\Delta H_{sol}/R$ (K)
CHASER	3.0e+5	3400
EMAC[a]	–	–
EMEP[b]	–	–
GIS MATRIX	1.e+2	3415
GISS OMA	1.e+2	3415
GMI	1.05e6	4200
INCA	7.4e+1	3400
Oslo-CTM2	3.3e+6	0
Oslo-CTM3	3.3e+6	0

1235 [a]EMAC: See its wet deposition description in section 4.1.1.
1236 [b]EMEP: The model does not use Henry law but applies simple empirical scavenging
1237 ratio, which for NH_3 is 1.4e6 for in-cloud and 0.5e6 for below-cloud scavenging. The
1238 scavenging ratio by definition is the ratio the concentration of a certain pollutant in
1239 precipitation divided by the concentration of the pollutant in air.
1240
1241
1242

Atmospheric
Chemistry
and Physics
Discussions

1243

1244 **Table 6. Baseline and three sensitivity experiments in the GMI model**

Experiment	Setup	Purpose
BASE	Standard simulation as described in section 2.1	Baseline simulation
TWET	Set NH_3 effective Henry law constant from 1.05e+6 (pH= 5.0) to 62 (pure water)	Review impact of NH_3 wet deposition
TnoNH3	Turn off NO_3^- production from NH_3/NH_4^+	Identify how large/where the NO_3^- formation from NH_3/NH_4^+
TnoHET	Turn off NO_3^- production from dust and sea salt	Identify how large/where the NO_3^- formation from dust and sea salt

1245

1246 **Table 7: NO_3^-, NH_4^+, NH_3 and HNO_3 budgets from the base simulation and three**
1247 **sensitivity experiments**

Tracer	Exps	Burden (Tg)	SConc (μg kg^{-1})	DDep (Tg a^{-1})	WDep (Tg a^{-1})	ChemDUSS (Tg a^{-1})	ChemP(Tg a^{-1})	Lifetime (days)
NO_3^-	BASE	0.26	0.22	14.9	31.5	41.9	4.8	2.1
	Twet	0.97	0.23	14.8	43.3	41.0	18.3	6.0
	TnoNH3	0.20	0.17	14.7	27.5	42.3	0	1.7
	TnoHET	0.099	0.065	0.61	6.70	0	7.1	5.0

1248

Tracer	Model	Emi (Tg a^{-1})	Burden (Tg)	SConc (μg kg^{-1})	DDep (Tg a^{-1})	WDep (Tg a^{-1})	ChemP/L (Tg a^{-1})	Lifetime (days)
NH_4^+	BASE		0.17	0.14	1.7	30.6	32.2	1.9
	Twet		0.48	0.16	1.9	50.7	53.0	3.4
	TnoNH3		-	-	-	-	-	-
	TnoHET		0.17	0.14	1.6	30.6	32.2	1.9
NH_3	BASE	60.4	0.11	0.40	12.6	17.5	30.4	0.67
	Twet		0.85	0.81	8.70	1.1	50.1	5.2
	TnoNH3		0.32	0.58	20.9	39.3	0	1.9
	TnoHET		0.10	0.40	12.6	17.4	30.4	1.2

1249

1250

1251

Atmospheric
Chemistry
and Physics
Discussions
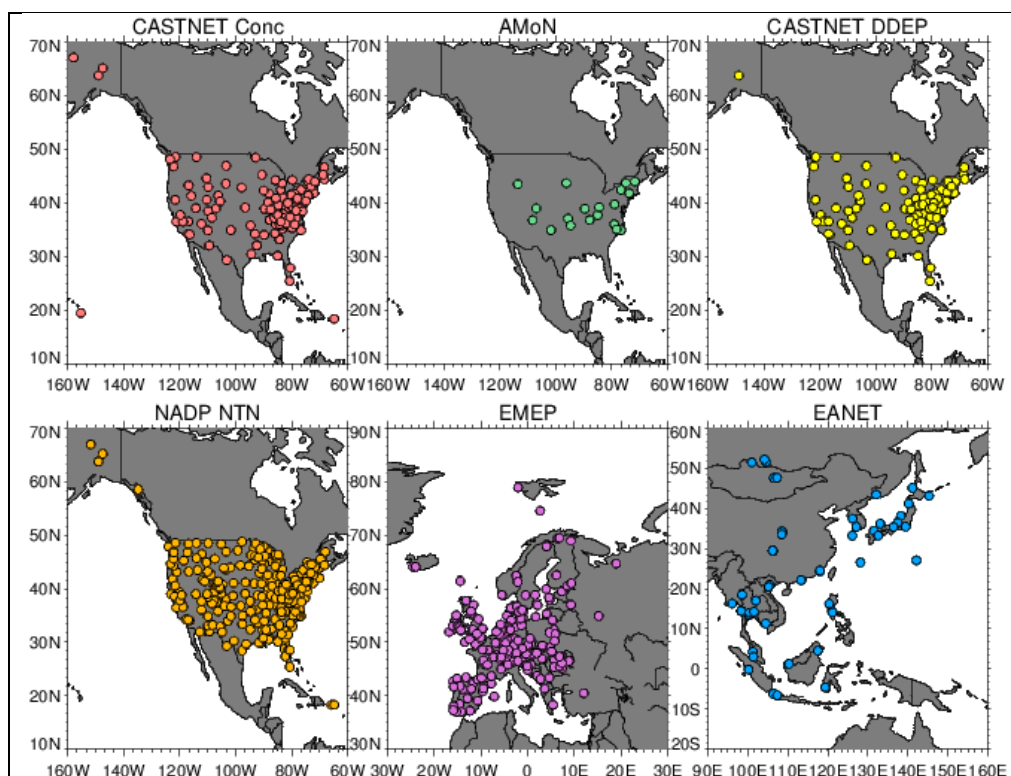
Figure 1. The observational station locations for CASTNET surface concentrations (CASTNET Conc), Ammonia surface monitor network over U.S. (AMON), CASTNET dry deposition (CASTNET DDEP); National Acid Deposition Network for wet deposition over U.S. (NADP NTN), surface concentrations over Europe (EMEP), and surface dry and wet deposition over Asia (EANET).

1252
1253
1254
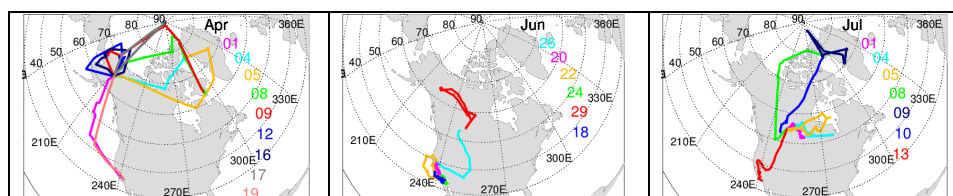
Figure 2. Flight-tracks of ARTCTA-A (left), ARCTAS-CARB (middle), and ARCTAS-B (right). The colors represent observations during different days.

1255

Atmospheric
Chemistry
and Physics
Discussions
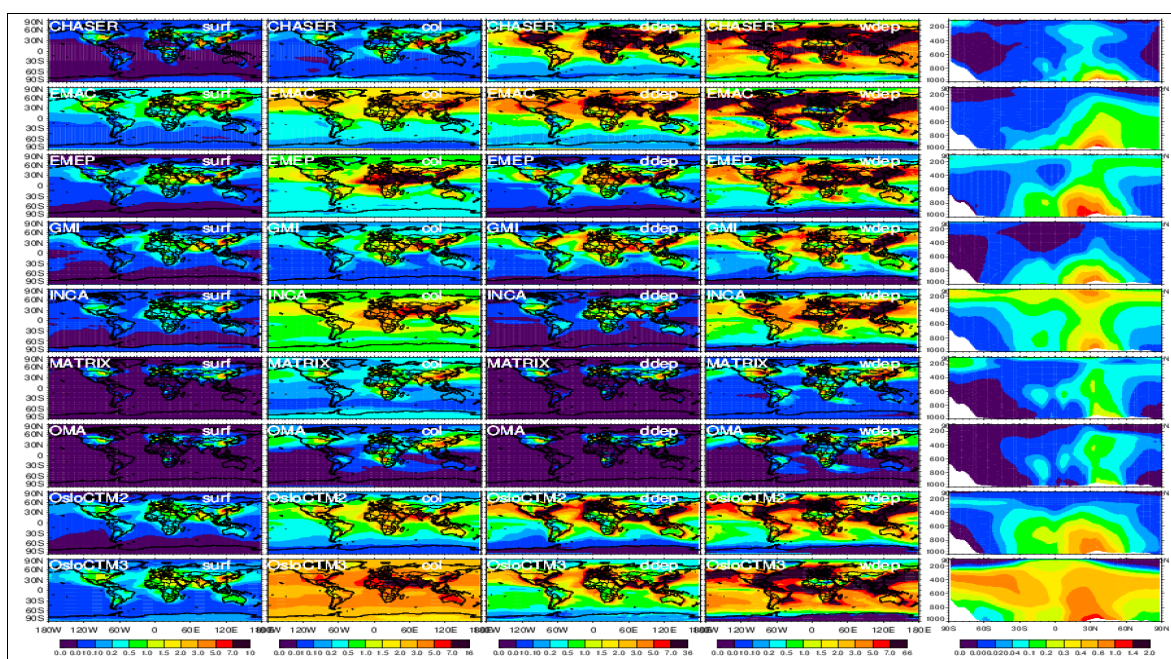
Figure 3a. Multimodel comparison of NO_3^- for surface mass mixing ratio (µg kg^{-1}, left), column load (mg m^{-2}, second), dry deposition (ng m^{-2} s^{-1}, third), wet deposition (ng m^{-2} s^{-1}, fourth), and vertical zonal mean (0.5µg kg^{-1}, right). Note that the CHASER dry and wet depositions and the EMAC wet deposition in this figure contain both NO_3^- and HNO_3, while the rest models NO_3^-.

Atmospheric
Chemistry
and Physics
Discussions

Open Access
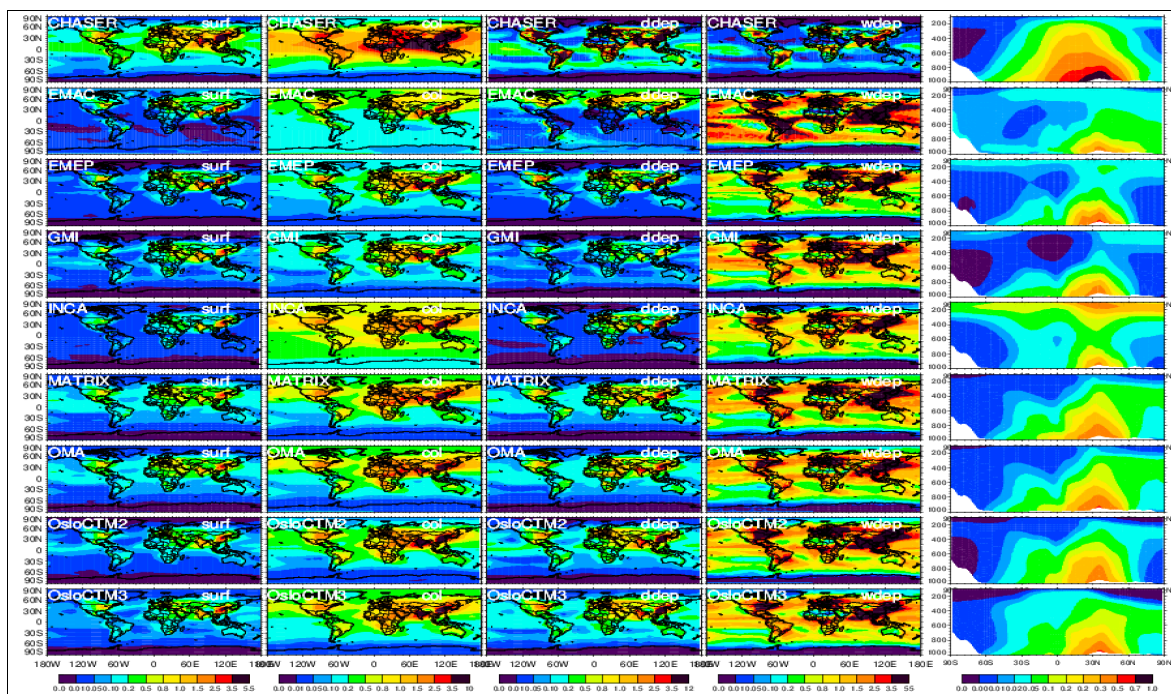
Figure 3b. Same as Figure 3a but for NH_4^+ and the unit in vertical distribution is µg kg^{-1}. Note that the EMAC wet deposition in this figure contain both NH_4^+ and NH_3, while the rest models only NH_4^+.

Atmospheric
Chemistry
and Physics
Discussions
Open Access

Figure 3c. Same as Figure 3a but for NH$_3$. Units are ppb for surface concentration and 0.1ppb for vertical distribution. Note that the EMAC wet deposition in this figure contain both NH$_3$ and NH$_4^+$, while the rest models only NH$_3$.
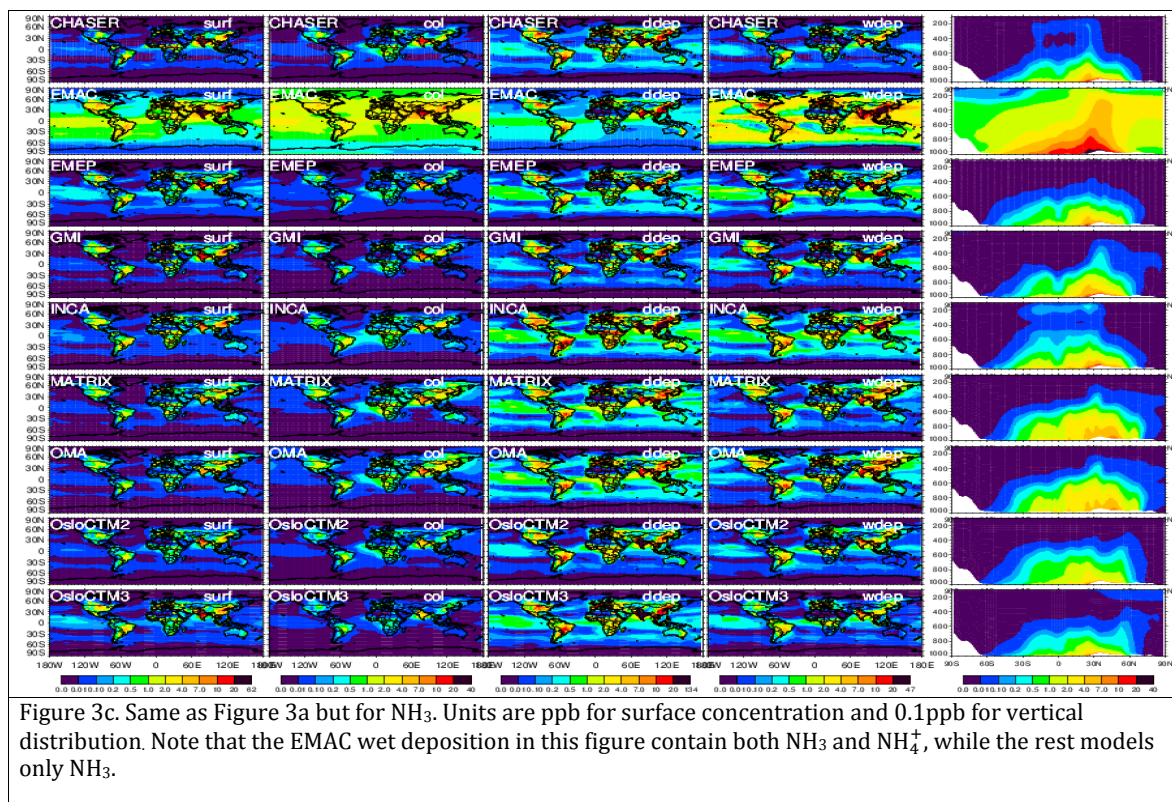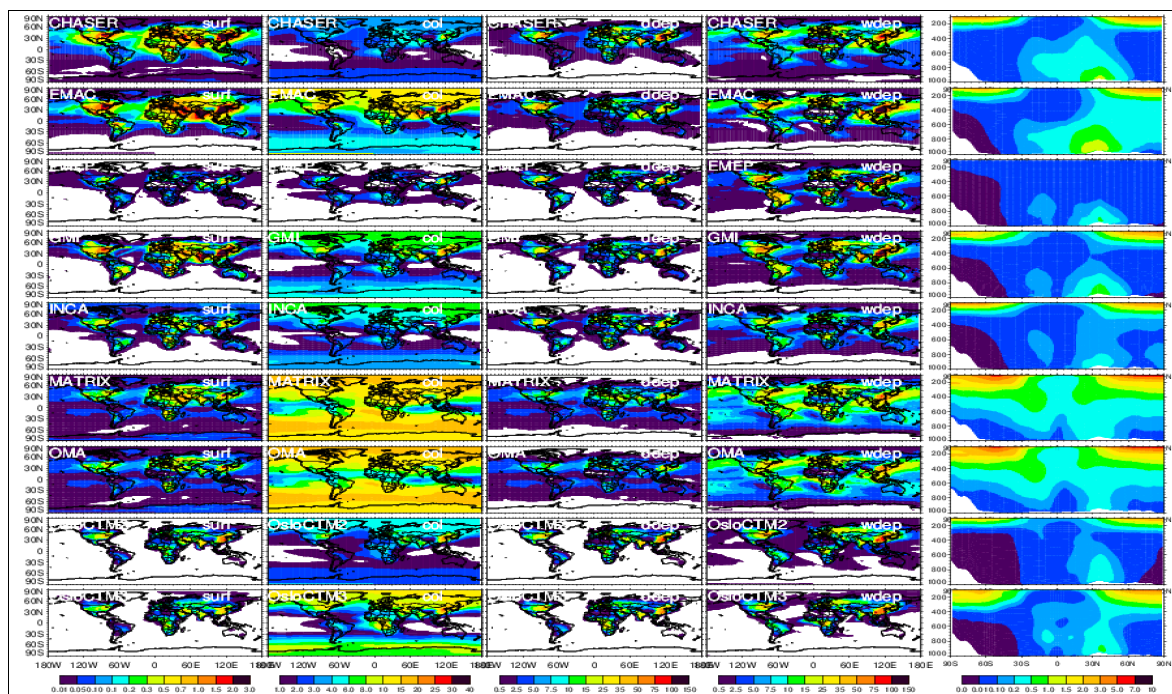
Figure 3d. Same as Figure 3a but for HNO_3. Units are 100 ppb for surface concentration, mg m^{-2} for loading, and 2ng m^{-2} s^{-1} for dry and wet depositions. Note that the column total of HNO_3 is from surface up to 100 ppb vertically. The CHASER dry and wet depositions and the EMAC wet deposition in this figure contain both HNO_3 and NO_3^-, while the rest models only HNO_3.

Figure 4a. Comparison of surface mixing ratios of NO_3^-, NH_4^+, NH_3, HNO_3, and SO_4^{2-} between models and CASTNET measurement. Units are µg m^{-3}.
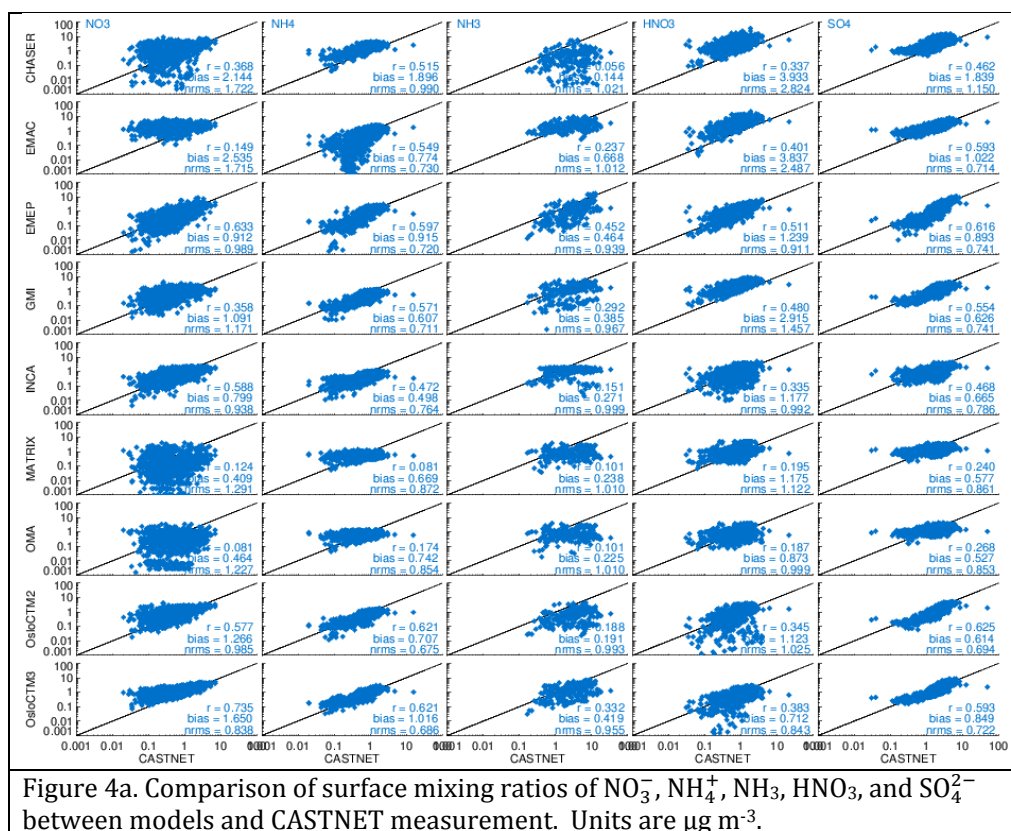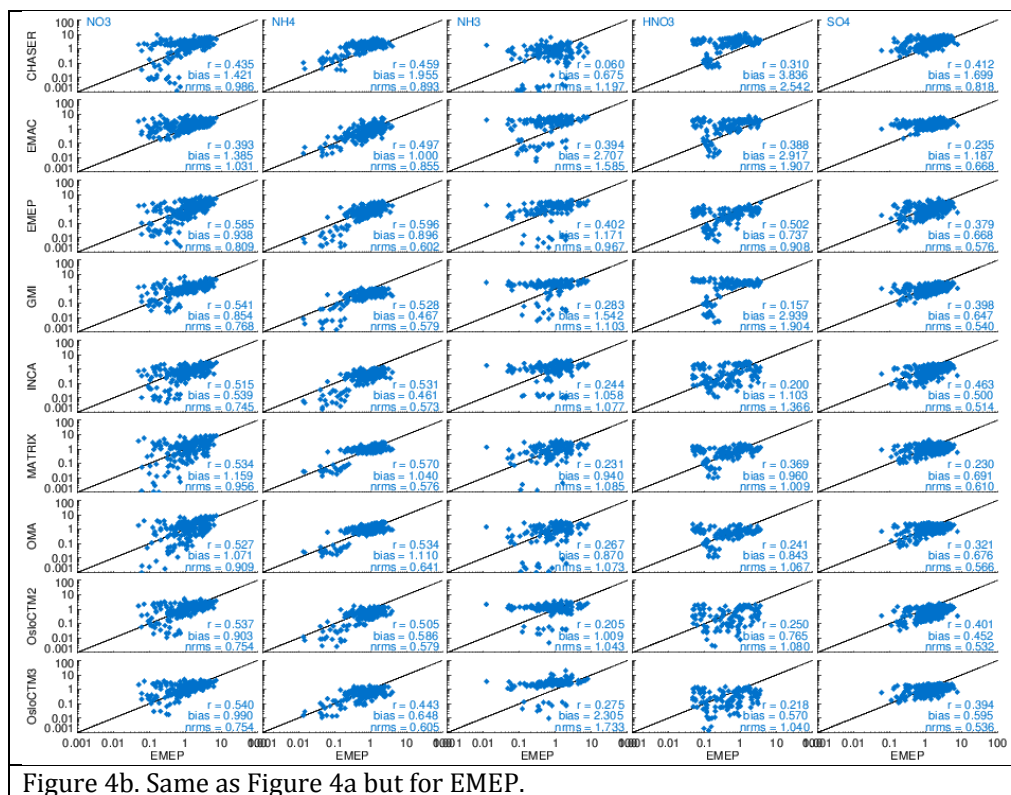
Figure 4b. Same as Figure 4a but for EMEP.
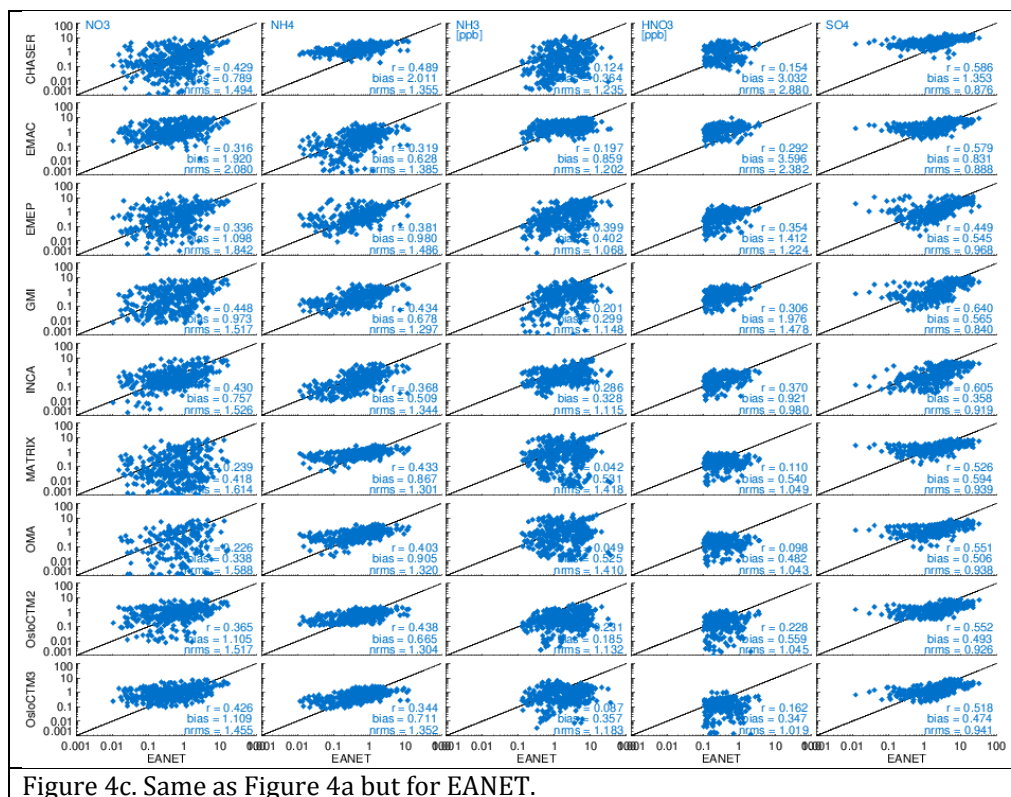
Figure 4c. Same as Figure 4a but for EANET.

Atmospheric
Chemistry
and Physics
Discussions
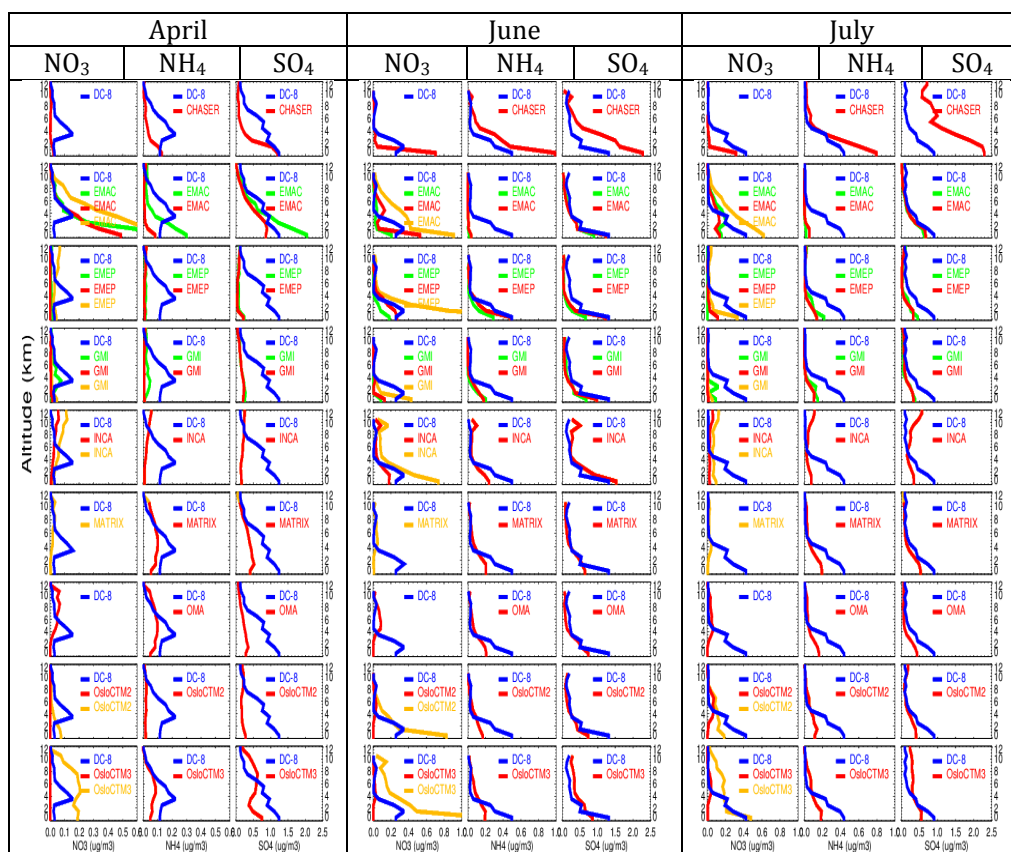
Figure 5. Vertical profile comparison between ARCTAS aircraft measurements and AeroCom model simulations. Note that ARCTAS AMS measurements give fine mode aerosols. Model profiles are shown in green (fine mode aerosol analyzed with daily output), red (fine mode aerosol with monthly output), and orange (total NO_3^- with monthly output). CHASER and OMA have fine mode NO_3^- only. Units are μg m^{-3}.

Figure 6. Comparison of surface dry deposition of NO_3^-, NH_4^+, HNO_3, and SO_4^{2-} between models and CASTNET measurements. Units are 10mg m^{-2} mon^{-1}.

Figure 7a. Comparison of surface wet deposition of NO$_3^-$+HNO$_3$, NH$_4^+$+NH$_3$, and SO$_4^{2-}$ between models and NDAP/NTN measurements. Units are 10mg m^{-2} mon^{-1}.

Figure 7b. Same as Figure 7a but for EANET with units of 100mg m^{-3}.

Figure 8. Zonal mean vertical distribution of NH_3 (0.01 ppb), NH_4^+ (0.1 μg kg^{-1}) and NO_3^- (0.05μg kg^{-1}) from base and three sensitivity experiments explained in Table 6.

Figure 9. Comparison between GMI simulations and ARCTAS measurements of NH_4^+ and NO_3^- from base and three sensitivity experiments explained in Table 6. Note the light blue line for $[NH_4^+]$ is frequently underneath the peak line.


Figure 10. NO_3^- fine mode burden (f-NO3, Tg), total burden (t-NO3, Tg), and coarse mode fraction (f_c) for the eight AeroCom models.